

Article

Multiprotein Inhibitory Effect of Dietary Polyphenol Rutin from Whole Green Jackfruit Flour Targeting Different Stages of Diabetes Mellitus: Defining a Bio-Computational Stratagem

Tejaswini Maradesha ¹, Shashank M. Patil ¹, Bhaskar Phanindra ², Raghu Ram Achar ³, Ekaterina Silina ⁴, Victor Stupin ⁵ and Ramith Ramu ^{1,*}

¹ Department of Biotechnology and Bioinformatics, JSS Academy of Higher Education and Research, Mysuru 570015, India

² Department of Pharmacology, JSS Medical College, JSS Academy of Higher Education and Research, Mysuru 570015, India

³ Division of Biochemistry, School of Life Sciences, JSS Academy of Higher Education and Research, Mysuru 570015, India

⁴ Institute of Biodesign and Modeling of Complex Systems, I.M. Sechenov First Moscow State Medical University (Sechenov University), 119991 Moscow, Russia

⁵ Department of Hospital Surgery 1, N.I. Pirogov Russian National Research Medical University (RNRMU), 117997 Moscow, Russia

* Correspondence: ramith.gowda@gmail.com; Tel.: +91-99-8638-0920; Fax: +91-82-1254-8394



Citation: Maradesha, T.; Patil, S.M.; Phanindra, B.; Achar, R.R.; Silina, E.; Stupin, V.; Ramu, R. Multiprotein Inhibitory Effect of Dietary Polyphenol Rutin from Whole Green Jackfruit Flour Targeting Different Stages of Diabetes Mellitus: Defining a Bio-Computational Stratagem. *Separations* **2022**, *9*, 262. <https://doi.org/10.3390/separations9090262>

Academic Editors: Jun Dang, Tengfei Ji and Xinxin Zhang

Received: 11 August 2022

Accepted: 13 September 2022

Published: 19 September 2022

Publisher's Note: MDPI stays neutral with regard to jurisdictional claims in published maps and institutional affiliations.



Copyright: © 2022 by the authors. Licensee MDPI, Basel, Switzerland. This article is an open access article distributed under the terms and conditions of the Creative Commons Attribution (CC BY) license (<https://creativecommons.org/licenses/by/4.0/>).

Abstract: The anti-diabetic potential of whole unripe jackfruit (peel with pulp, flake, and seed) was investigated using inhibitory assays for α -glucosidase, α -amylase, aldose reductase, and glycation at multiple stages. Using activity-guided repeated fractionation on a silica gel column chromatography, dietary flavonoid rutin with potent antihyperglycemic activity was extracted from the methanol extract of whole jackfruit flour (MJ). Rutin was found to inhibit both α -glucosidase (IC_{50} : 7.86 μ g/mL) and α -amylase (IC_{50} : 22.00 μ g/mL) in a competitive manner of inhibition with low K_i values. In addition, in vitro glycation experiments revealed that rutin prevented each stage of protein glycation as well as the production of intermediate molecules. Furthermore, rutin significantly inhibited aldose reductase (IC_{50} : 2.75 μ g/mL) in a non-competitive manner. During in silico studies, molecular docking and molecular dynamics simulation studies have suggested that rutin has a high binding affinity for the enzymes studied, which could explain its inhibitory effects. Rutin interacted with the key residues of the target enzymes' inhibitor binding sites. Compared to the controls used, rutin had a higher binding efficiency as well as stability in the inhibitor binding pocket of the target enzymes. According to our findings, the presence of rutin is more likely to be associated with the potential of MJ in antihyperglycemic activity via inhibition of α -glucosidase and in anti-diabetic action via inhibition of the polyol pathway and protein glycation. The bio-computational study indicates rutin as a potential lead inhibitor of all the target enzymes used and could be used as an effective anti-diabetic drug in the near future.

Keywords: whole jackfruit; diabetes mellitus; dietary flavonoid; rutin; inhibition kinetics; molecular dynamics simulation; phyto-computational stratagem

1. Introduction

Type 2 diabetes mellitus (T2DM) is regarded as a serious concern of endocrine health, where altered body metabolism occurs due to an imbalance in insulin levels [1]. Over the past few decades, diabetes and obesity have increased at an unprecedented rate, affecting more than 10.5% and 13%, respectively, of the global adult population. In addition, it is also recognized as a pediatric medical problem [2,3]. In >90% of all instances, T2DM is reportedly more common than T1DM. There have been a few instances of it in children and teenagers, but adults are the ones who typically experience it [4]. Due to the increasing

levels of fast urbanization, poor diets, tobacco consumption, obesity, environmental factors, aging populations, and sedentary lifestyles, the condition continues to pose a global danger [5]. Diabetes mellitus patients may develop a number of concomitant health maladies known as diabetic complications as a result of chronic hyperglycemia and insulin resistance. These include persistent deterioration and the dysfunction of bodily tissues, which results in diabetes cardiomyopathy, nephropathy, neuropathy, retinopathy, and diseases of the liver, pancreas, adipose tissue, and skeletal muscle [6].

The pathophysiology of diabetes mellitus is spread throughout different stages of human metabolism. Most of the events related to the development of diabetic conditions occur during the absorption of digested food. For instance, glycoside hydrolases are known as α -glucosidase (AG) and α -amylase (AM), which aid in the swift digestion of ingested carbohydrates into simpler monosaccharides, resulting in postprandial hyperglycemia (excess blood glucose). This is the first sign of diabetes, and glycoside inhibitors are widely acknowledged as an effective way to control postprandial hyperglycemia by preventing the release of free sugars, allowing for a stable glycemic profile [7,8].

By the action of aldose reductase (AR), high blood glucose levels produce a substantial flux of glucose into the polyol pathway, where it is converted to sorbitol [7,9]. Reduced metabolism or decreased membrane permeability of sorbitol dehydrogenase causes the overproduction of sorbitol, which in turn accumulates in tissues, such as nerves, retina, kidney, retina, and lens. Therefore, AR can act as a crucial target, which can be inhibited to prevent sorbitol accumulation, which is linked to a variety of microvascular problems and cardiovascular disorders [10]. In addition, protein glycation in diabetes mellitus results in a partial loss of activity as a result of persistent hyperglycemia. A non-enzymatic nucleophilic addition reaction of the carbonyl residue of sugar with the free amino group of proteins produces a reversible Schiff base, which ultimately yields a more stable Amadori product. The Amadori products are subsequently exposed to a series of dicarbonyl intermediate-mediated processes, yielding an unknown family of molecules known as advanced glycation end products (AGEs). These AGEs accumulate in tissues and are the source of micro- and macro-vascular problems in diabetics [11,12].

As a result, finding molecules that block all the stages of glycation and the synthesis of intermediary products in the route can aid in the development of new therapeutic approaches to delay or avoid harmful consequences. Furthermore, by interfering with the signal transduction cascade, glycated proteins and AGEs cause the production of reactive oxygen species (ROS), resulting in oxidative stress, which is a key factor in the advancement of numerous vascular problems in diabetes [11]. Antioxidants, which neutralize the produced free radicals, are the most effective way to defend against ROS-mediated damage. Overall, a medication with integrated antioxidant and anti-glycation characteristics, as well as potent AG inhibition and reduced AM inhibition, may be the most effective treatment for diabetes mellitus and its consequences [13].

In this context, the use of fruits and vegetables to prevent diabetes has been the center of focus. The effects exerted are mainly due to the enormous antioxidant and antihyperglycemic potentials present in fruits and vegetables, which indicates the pharmacological potential of phytochemicals to curb diabetes mellitus. [14,15]. Diabetes mellitus is a chronic metabolic syndrome produced by a shift in diet and lifestyle from traditional diets rich in plant-based foods, including legumes, grains, fruits, and vegetables, to more Western-style diets rich in fat, carbohydrates, and animal-source foods [16,17]. Therefore, traditional diets rich in bioactive compounds are indeed an effective mode of therapy to achieve long-term control of diabetes. Thus, the present era can be marked as the period of transition providing a better scientific basis for phytochemical therapies. It also paves newer avenues to the modern understanding of dietary interventions known as non-pharmacological interventions, in the treatment of chronic diseases such as diabetes mellitus [18,19].

To date, several plant species have been investigated for their anti-diabetic potential against multiple targets. *Artocarpus heterophyllus* (jackfruit), a member of the *Moraceae* family and a common household tree in India and Bangladesh, is the most well-known

of these species. This tree is very popular for its fruit and timber and is commonly called “the poor man’s food” because of its abundance and lower cost [20]. Studies have proved that the fruit contains carotenoids, flavonoids, volatile acids, sterols, and tannins with a robust antioxidant potential [20,21]. Although information is available on ripe jackfruit in terms of its composition and health benefits, there is scarce knowledge on its potential in the treatment of diabetes [20,22].

Therefore, we aim to investigate the anti-diabetic potential of methanol extract of whole unripe jackfruit flour (MJ) by inhibiting AG and AM, which cause hyperglycemia. We also aim to evaluate its effect on AR and protein glycation, which cause numerous diabetic complications. Glycation indicators were evaluated at each stage of glycation, including fructosamines (early stage), protein carbonyls (middle stage), and AGEs (late stage). Moreover, the isolation of active compounds responsible for the beneficial properties followed by computational approaches to evaluate their druggability and ability to bind to the target proteins was also carried out.

2. Materials and Methods

2.1. Plant Material

In May 2019, whole mature and unripe jackfruits (94–101 days) were collected in Chandra Bakke cultivar nurturing farms of Nanjangud, Karnataka, India (geographical coordinates: 12°9′12.88″ North 76°42′51.01″ East), and authenticated (MYS 457869) by the Department of Horticulture, Government of Karnataka, Mysore, India, which also housed voucher specimens. Before being sliced into bits, the samples were rinsed under running tap water. They were then shade-dried before being milled into flour and kept at 4 °C until needed.

2.2. Extraction

Using the Soxhlet apparatus (Borosil, Mumbai, Maharashtra, India), crude extracts of whole jackfruit flour were obtained by extracting 500 g of dried whole jackfruit (peel with pulp, flake, and seed) with solvents of increasing polarity (chloroform, ethyl acetate, acetone, methanol, and water). The solvents used for extraction were of analytical grade (99%) and were procured from Merck (Mumbai, India). The methanol extract was selected for further studies as it was found to be more active on the basis of antioxidant and anti-diabetic potential. The yield of the crude methanol extract was 70 g. This crude extract was fractionated using a series of column chromatography into petroleum ether, ethyl acetate, and n-butanol fractions. The active ethyl acetate soluble fraction was chromatographed on a silica gel column and successively eluted with stepwise linear gradients of chloroform:methanol. The most active fraction (90:10) was further chromatographed on a Sephadex LH-20 column (Mitsubishi Chemical Corporation, Tokyo, Japan) with methanol solvent to obtain rutin (Supplementary Materials Figure S1).

2.3. Inhibition Assay and Kinetics for AM, AG, and AR Inhibitory Activity

The crude extracts, fractions, and isolated rutin were evaluated for anti-diabetic target enzyme inhibition (AM, AG, and AR). All the test samples (crude extracts, fractions, and rutin) with varying concentrations (0–1000 µg/mL) were dissolved in dimethyl sulfoxide. Acarbose (AG and AM) and quercetin (AR) were used as the positive controls. The inhibition tests for AM (EC 3.2.1.1, type-VI B porcine pancreatic amylase), yeast AG (EC 3.2.1.20, type-1 α-glucosidase), and human recombinant AR were performed using starch (1%), pNPG (0.5 mM), and DL-glyceraldehyde (5 mM), respectively, as described earlier [7]. By comparing the absorbance change of the test samples to that of the control, the inhibitory activity was assessed. Using the formula below, the results were reported as a percentage of enzyme inhibition (AM, AG and AR).

$$\text{Inhibition (\%)} = \frac{A_{(\text{control})} - A_{(\text{sample})}}{A_{(\text{control})}} \times 100$$

Each experiment was carried out three times with the necessary blanks. The inhibitory activity of the test samples were represented by the least-squares regression line of logarithmic concentrations plotted against percent inhibition, which yielded the IC_{50} values ($\mu\text{g/mL}$). When compared to the control, this number (IC_{50} values) shows the concentration of test samples that can inhibit enzyme activity by 50%. The inhibition kinetics of AM, AG, and AR were determined using the method described by Maradesha et al. (2022) [20].

2.4. Assay for Antioxidant Activity

According to a previous study by Razali et al., 2008 [23], the antioxidant activity was assessed under in vitro conditions using the DPPH (2,2-diphenyl-1-picryl-hydrazyl-hydrate), superoxide, and ABTS (2,2'-azino-bis(3-ethylbenzothiazoline-6-sulfonic acid)) radical scavenging activities. The tests were conducted in triplicates. Their potential radical scavenging capability was represented by EC_{50} values. An EC_{50} value implies scavenging of 50% of free, cation, and anion radicals.

2.5. Analysis of Phenolic Compounds and Ascorbic Acid by HPLC

With a few minor modifications in the protocol, the identification of phenolic compounds from methanol extract of whole jackfruit flour (MJ) was conducted according to Seal (2016) [24]. With a photodiode array (PDA) detector and a reverse phase C18 (250 mm 4.6 mm, Supelco) column, the HPLC system (Agilent Technologies, Santa Clara, CA, USA) was run at 37 °C with a flow rate of 0.8 mL/min and an injection volume of 20 μL . Methanol (solvent A) and 0.1% formic acid (*v/v*) in water (solvent B) made up the mobile phase. From 0 to 55 min, the elution gradient was 85% A and 15% B; from 55 to 57 min, 20% A and 80% B; from 57 to 60 min, 85% A and 15% B. The phenolic compounds peak areas were compared to those of the standards viz. ascorbic acid, gallic acid, catechin, methyl gallate, caffeic acid, syringic acid, rutin, p-coumaric acid, sinapic acid, ferulic acid, myricetin, quercetin, apigenin, and kaempferol (Supplementary Materials Figure S2).

2.6. Determination of Total Flavonoid Content (TFC) and Total Phenol Content (TPC)

The TFC was evaluated using a modified protocol by Ordon et al. (2006) [25]. Furthermore, 200 μL of a 0.5 mol/L sodium carbonate solution was mixed with one milliliter of MJ of different concentrations (0–1000 $\mu\text{g/mL}$). The mixture was added to 200 μL of 0.3 mol/L aluminum chloride crystalline after standing for 5 min, and the mixture was then incubated for an additional 5 min. The reaction system was then added with 1.0 mL of 1 M NaOH, and the absorbance was measured at 510 nm in comparison to a blank. Quercetin equivalents per gram of dry weight (QE/g) were used to calculate and express the results.

By the Folin–Ciocalteu method, the TPC in MJ was determined as per Shuxia et al. (2013) [26]. In brief, 5.9 mL of water was used to dilute MJ (100 μL) of different concentrations (0–1000 $\mu\text{g/mL}$) before they were mixed. In addition, 200 μL of Folin–Ciocalteu reagent was added, and 2 mL of sodium carbonate solution was added 1 min later to the mixture. A 120-min reaction at room temperature and dark conditions was given to the mixture before the absorbance at 735 nm was obtained. Results were represented in milligrams of gallic acid equivalents (GAE/g) and compared to a reference of gallic acid.

2.7. Separation and Identification of Rutin

The methanol extract was chosen for the extraction of bioactive constituents because of its inhibitory potential (AG, AM, and AR), yield, and antioxidant capabilities. The methanol extract of whole jackfruit flour (MJ) was subjected to phytochemical profiling [27]. First, 70 g of MJ was fractionated using column chromatography (90 cm \times 3 cm) on silica gel (100–200 mesh) and eluted with analytical grade (99%) solvents such as ethyl acetate, petroleum ether, and n-butanol (500 mL). Next, the soluble fractions (petroleum ether: 7 g; ethyl acetate: 8 g; n-butanol: 6 g) were collected (21 fractions), concentrated (flash evaporation), and then tested for anti-diabetic and antioxidant activities. The active ethyl acetate soluble fraction (Fr. I-09–15) was chromatographed once more on a silica gel

column (35 cm × 2 cm) and successively eluted with stepwise linear gradients of chloroform: methanol (100:0; 95:5; 90:10; 80:20; 75:25; 50:50; 25:75; 0:100 *v/v*). Then, the fractions were gathered (51 fractions) and spotted on Merck's F254 pre-coated silica gel plates (20 × 20 cm). The optimum resolution was obtained in the solvent system of ethyl acetate: toluene: formic acid (4.5:5:0.5, *v/v*). Thin Layer Chromatography (TLC) plates were subjected to iodine fumes to visualize the spot. The fractions (Fr) in the TLC pattern that had a similar retention factor (*R_f*) were combined. The anti-diabetic and antioxidant activity of these fractions were evaluated. The most active ethyl acetate soluble fraction Fr. II (37–42) was again separated using silica gel column (30 cm × 2 cm) chromatography with a 90:10 mixture of chloroform and methanol, followed by re-chromatography using a Sephadex LH20 column with methanol as the eluting solvent to yield rutin (Supplementary Material Figure S1). Rutin (96 mg) was isolated from Fr. II (37–42) with a single spot-on TLC with ethyl acetate: toluene: formic acid (4.5:5:0.5, *v/v*) as the mobile phase.

2.8. Structural Elucidation

Fourier transform infrared (FT-IR) (Thermo Fisher Scientific, Rockford, IL, USA), LCMS2010A (Shimadzu, Tokyo, Japan), and the ¹H and ¹³C Nuclear magnetic spectrometer (NMR) (Bruker Biospin Co., Karlsruhe, Germany) with deuterated chloroform or chloroform-d (CDCl₃) as a solvent were used to determine the chemical structure of rutin.

2.9. Multiple Stages of the Human Serum Albumin (HSA) Glycation Inhibition Assay

The antiglycation potential of rutin was examined at multiple stages, namely early glycation product (fructosamine), intermediate (protein carbonyls), and late-stage glycation end products (AGEs), according to the procedure published in our previous work [1].

2.10. Molecular Docking Simulation

Protein and ligand preparation, binding site prediction, and virtual screening of the phenolic compounds were conducted according to Patil et al. (2021) [28]. The AG protein sequence retrieved from UniProt (<https://www.uniprot.org/>) was used to construct a homology model using SWISS-MODEL (<https://swissmodel.expasy.org/> accessed on 10 July 2022). The protein model was constructed using an x-ray crystal structure of *Saccharomyces cerevisiae* isomaltase (PDB ID: 3AXH), which showed 72% identical and 84% comparable sequences at a resolution of 1.8 Å [29]. The validation of protein structure using the Ramachandran plot revealed the presence of 94% of the 9362 residues in favorable regions [28]. In addition, the X-ray crystal protein structures of AM (PDB ID: 1DHK), human serum albumin (HSA) (PDB ID: 2BXG), and human AR (HAR) (PDB ID: 1IEI) were obtained from the RCSB PDB database (<https://www.rcsb.org/> accessed on 10 July 2022). For these proteins, the binding site was predicted using the literature analysis. For AG, the binding site predicted in the previous study was used [22]. Binding pocket of AG was placed in a box of 40 Å × 40 Å × 40 Å positioned at *x* = −17.489 Å, *y* = −8.621 Å, and *z* = −19.658 Å using AutoDock Tools 1.5.6 (Center for Computational Structural Biology Logo) [28]. Similarly, for AM (22.48 Å × 22.48 Å × 22.48 Å positioned at *x* = 103.469 Å, *y* = 37.176 Å, *z* = 19.607 Å), HSA (15.02 Å × 15.02 Å × 15.02 Å positioned at *x* = 8.249 Å, *y* = 2.58 Å, and *z* = −14.75 Å), and HAR (8.25 Å × 8.25 Å × 8.25 Å positioned at *x* = −5.06 Å, *y* = 0.19 Å, and *z* = 9.94 Å), grid boxes consisting of binding residues were placed. In case of ligand preparation, phytochemical structures in 3D Spatial Data File (SDF) format obtained from PubChem (<https://pubchem.ncbi.nlm.nih.gov/> accessed on 11 July 2022) were converted into PDBQT format using OpenBabel 2.3.1 [30]. After ligand preparation, the compounds were docked into their respective protein targets using AutoDock Vina 1.1.2. Acarbose was used as a control for both AG and AM, whereas aminoguanidine and quercetin were used as a control for HSA and HAR, respectively.

2.11. Molecular Dynamics Simulation

The docked conformations of target proteins and respective ligands with the most negative binding affinity were selected, and the molecular dynamics simulation was performed according to Patil et al. (2021) [31]. The GROMACS-2018.1 software package (The Biophysical Chemistry department of University of Groningen, Groningen, Poland) was used for the simulation [32]. The CHARMM36 force field was applied to all the protein–ligand complexes, subsequently obtaining the ligand topology using the CGenFF server [33]. Using the GROMACS pdb2gmx module, hydrogen atoms were added to the present heavy atoms. Subsequently, vacuum minimization of 5000 steps was performed utilizing the steepest descent algorithm. Both protein–rutin and protein–acarbose complexes were placed in a box of 10 Å distance to the edges. The solvent was added using the TIP3P water model. Further, by incorporating the appropriate number of Na⁺ and Cl[−] counter ions, all the systems were neutralized. The steepest descent and conjugate gradient methods were employed to minimize the energy of the systems. A short equilibration in constant number (N), volume (V), and temperature (T) or NVT and constant number (N), pressure (P), and temperature (T) or NPT ensembles (1000 ps each) were performed prior to the simulation run. In total, 12 simulations were run (4 bare protein atoms, 4 protein–rutin complexes, and 4 protein–standard drug complexes) for 100 ns time at 310K temperature and 1 bar pressure. The protein–ligand root-mean-square deviation (RMSD), root-mean-square fluctuation (RMSF), radius of gyration (Rg), and solvent accessible surface-area trajectory analysis (SASA) and ligand hydrogen bond trajectory analysis were conducted by plotting the respective graphs using XMGRACE 5.1.22 [34].

2.12. Binding Free Energy Calculations

Another application of molecular dynamics simulations and thermodynamics to analyze the extent of ligand binding with protein is the computation of binding free energy of a protein–ligand complex. The Molecular Mechanics/Poisson–Boltzmann Surface Area (MM-PBSA) technique was employed to calculate the binding free energy for each ligand–protein complex using the g_mmpbsa tool [35]. The binding free energy is calculated using three components in the g_mmpbsa tool: molecular mechanical energy, polar and apolar solvation energies, and molecular mechanical energy. The last 50 ns of molecular dynamics trajectories were used to compute ΔG with dt 1000 frames. The binding free energy is computed using Equation (1) below, while the free energy of individual complex components is obtained using Equation (2) below:

$$\Delta G_{\text{binding}} = G_{\text{complex}} - (G_{\text{protein}} + G_{\text{ligand}}) \quad (1)$$

$$G = (E_{\text{MM}}) - TS + (G_{\text{sol}}) \quad (2)$$

$$E_{\text{MM}} = E_{\text{bonded}} + E_{\text{nonbonded}} \quad (3)$$

$$G_{\text{sol}} = G_{\text{polar}} + G_{\text{nonpolar}} \quad (4)$$

G_{sol} is the sum of the solvation-free energy, while E_{MM} is the average potential energy in vacuum. E_{bonded} indicates the bond length, angle, and torsion angle in Equation (3), whereas non-bonded van der Waals and electrostatic are observed in Equation (3). The energy required to transport a solute from vacuum to a solvent is calculated using Equation (4). The electrostatic and non-electrostatic support for the solvation-free energy is represented by G_{polar} and G_{nonpolar} [36].

2.13. Statistical Analysis

All three different sets of experiments were conducted in triplicates. The data is presented as a mean standard deviation (mean \pm SE). The computer program SPSS 21.0 version for Windows (Version 21.0, Chicago, IL, USA) was used for statistical analysis. Duncan's multiple range tests were performed to establish the study's significance, followed by one-way ANOVA. The level of statistical significance was chosen at $p \leq 0.05$.

3. Results

3.1. Isolation and Identification of Rutin from MJ

The methanol extract was chosen for extraction and purification of the bioactive component responsible for whole jackfruit flour due to its high antioxidant and anti-diabetic potential (Table 1) in comparison to other solvents (viz. chloroform, ethyl acetate, acetone, and water). Further, the crude methanol extract was fractionated chromatographically into three different polarity extracts: petroleum ether, ethyl acetate, and n-butanol. Individual soluble fractions were then tested for radical scavenging activities (DPPH, ABTS, and superoxide) and enzyme inhibition (AG, AM, and AR) to calculate the anti-diabetic as well as antioxidant effects of the extract fractions. Ethyl acetate was found to be the most effective solvent (in comparison to petroleum ether and n-butanol) in radical scavenging and anti-diabetic activities, with the lowest IC₅₀ and EC₅₀ values (Table 1). The findings suggest that bioactive components derived from whole jackfruit flour are more abundant in the ethyl acetate fraction of the methanol extract. Using column chromatography, the bioactive component of the ethyl acetate fraction from whole jackfruit flour was extracted (Supplementary Figure S1).

Table 1. Antioxidant activity and inhibitory potential of crude extracts and its respective fractions of green jackfruit flour against α -amylase, α -glucosidase, and aldose reductase enzymes.

Extracts (Ext./Fractions (Fr.))	Enzyme Inhibition IC ₅₀ ^{x,y} (μ g/mL)			Antioxidant Activity EC ₅₀ ^{x,z} (μ g/mL)		
	α -Amylase	α -Glucosidase	Aldose Reductase	DPPH	ABTS	Superoxide
Chloroform (Ext.)	43.00 \pm 0.86 ^h	24.09 \pm 0.14 ^f	9.00 \pm 0.15 ^d	35.65 \pm 0.57 ^h	35.14 \pm 1.25 ^h	66.25 \pm 1.19 ⁱ
Ethyl Acetate (Ext.)	36.65 \pm 0.14 ^f	15.00 \pm 0.88 ^e	9.68 \pm 1.11 ^e	37.05 \pm 1.23 ⁱ	32.00 \pm 0.00 ^g	50.80 \pm 0.08 ^f
Acetone (Ext.)	31.00 \pm 0.50 ^e	14.45 \pm 0.23 ^e	8.00 \pm 0.04 ^d	30.66 \pm 0.08 ^f	28.00 \pm 0.94 ^f	52.99 \pm 0.37 ^g
Methanol (Ext.)	27.95 \pm 0.10 ^c	10.10 \pm 0.20 ^c	3.80 \pm 1.01 ^b	24.55 \pm 1.52 ^d	21.00 \pm 0.96 ^c	44.75 \pm 1.23 ^e
Water (Ext.)	47.00 \pm 0.86 ⁱ	31.15 \pm 0.08 ^g	10.20 \pm 1.41 ^e	44.50 \pm 0.02 ^k	36.65 \pm 0.10 ^h	57.88 \pm 1.33 ^h
Petroleum ether (Fr.)	40.50 \pm 1.44 ^g	30.50 \pm 0.54 ^g	8.50 \pm 0.30 ^d	32.50 \pm 0.11 ^g	39.15 \pm 0.88 ⁱ	57.00 \pm 1.00 ^h
Ethyl Acetate (Fr.)	26.15 \pm 0.15 ^c	09.00 \pm 0.10 ^b	3.25 \pm 0.70 ^b	23.50 \pm 0.35 ^d	19.06 \pm 1.74 ^b	40.75 \pm 0.65 ^d
n-butanol (Fr.)	31.00 \pm 0.77 ^e	14.50 \pm 0.55 ^e	6.00 \pm 1.01 ^c	28.50 \pm 0.80 ^e	25.00 \pm 0.90 ^e	46.14 \pm 1.26 ^e
Cf:Me (22–30)	28.00 \pm 0.34 ^c	12.00 \pm 1.33 ^d	5.50 \pm 0.33 ^c	27.05 \pm 0.12 ^e	23.00 \pm 0.12 ^d	41.50 \pm 1.14 ^d
Cf:Me (31–36)	27.88 \pm 1.87 ^c	10.75 \pm 1.02 ^c	5.25 \pm 0.55 ^c	27.10 \pm 1.09 ^e	22.15 \pm 1.73 ^c	37.75 \pm 1.00 ^c
Cf:Me (37–42)—Rutin	22.00 \pm 0.16 ^a	07.86 \pm 0.33 ^a	2.75 \pm 0.10 ^a	15.00 \pm 0.18 ^a	10.70 \pm 0.47 ^a	27.05 \pm 1.00 ^a
Cf:Me (43–48)	25.00 \pm 0.00 ^b	09.05 \pm 0.40 ^b	6.33 \pm 0.21 ^c	18.25 \pm 1.88 ^b	18.55 \pm 1.11 ^b	30.30 \pm 0.04 ^b
Cf:Me (49–54)	28.20 \pm 1.33 ^c	10.50 \pm 0.66 ^c	6.00 \pm 0.12 ^c	25.10 \pm 1.01 ^d	25.40 \pm 0.75 ^e	40.06 \pm 0.15 ^d
Cf:Me (55–60)	28.13 \pm 0.07 ^c	09.50 \pm 1.10 ^b	6.50 \pm 0.00 ^c	19.20 \pm 1.02 ^c	20.65 \pm 1.66 ^c	40.00 \pm 0.26 ^d
Cf:Me (61–66)	27.77 \pm 1.19 ^c	08.80 \pm 0.56 ^b	5.05 \pm 1.00 ^c	20.20 \pm 1.08 ^c	23.35 \pm 0.68 ^d	35.66 \pm 0.14 ^c
Cf:Me (67–72)	28.75 \pm 0.55 ^d	10.88 \pm 0.16 ^c	3.90 \pm 0.16 ^b	34.66 \pm 0.09 ^h	26.11 \pm 0.54 ^e	50.00 \pm 0.44 ^f
Positive control *	29.00 \pm 0.16 ^d	11.05 \pm 0.23 ^c	4.00 \pm 0.14 ^b	40.00 \pm 0.18 ^j	31.25 \pm 0.02 ^g	65.00 \pm 0.10 ⁱ

^x Values are reported as mean \pm SE. A significant variation between the extracts and fractions is indicated by the different superscript letters (a–k) are significantly different ($p \leq 0.05$) according to Duncan multiple range test. ^y The IC₅₀ (μ g/mL) value is the sample concentration at which 50% inhibition was achieved. ^z The effective concentration of samples required to show 50% antioxidant activity under assay conditions is defined as the EC₅₀ (μ g/mL) value. * In the α -amylase and α -glucosidase inhibition assays, acarbose was utilized as a positive control, but in the aldose reductase assay, quercetin was employed as a positive control.

The bioactive compound was characterized as rutin with the resulting characteristics: pale yellow amorphous powder. Melting point: 242 °C. UV (methanol): λ_{max} 359 nm. IR (KBr): 3520–3610 cm⁻¹ (OH). ¹H NMR (DMSO): δ 1.21 (s, 3H, CH₃), 3.48 (m, 6H, 6-HO-CH), 3.75 (d, 2H, O-CH₂), 3.9 (d, 1H, -O-CH), 4.15 (bs, 6H, 6-OH), 4.2 (q, 1H, -O-CH-C), 5.1 (s, 2H, 2-O-CH), 5.55 (bs, 4H, 4-OH), 6.2–6.6 (m, 5H, Ar-H). ¹³C NMR (DMSO): δ 16.8, 64.5, 70.6, 71.8, 73.2, 73.5, 73.6, 73.9, 75.9, 77.7, 92.7, 98.0, 98.3, 104.5, 105.5, 113.6, 117.2, 120.4, 124.4, 135.1, 146.5, 147.2, 154.9, 160.1, 163.9, 166.4, 178.3. MS: m/z 611 (M+1). Analytical calculated data for C₂₇H₃₀O₁₆ (610.15): C, 53.12; H, 4.95. Found: C, 53.15; H, 4.93%. On the basis of the previously mentioned findings (Supplementary Materials Figures S3 and S4), as well as comparisons with NMR and MS data in the literature, the identity of rutin was determined [37,38]. These results concur with our HPLC findings that rutin was found

in the methanol extract (Table 2). Additionally, the total phenolic content (253.7 mg GAE per g) and total flavonoid content (602.20 mg QE per g) of MJ was found to be high.

Table 2. HPLC study of phenolic components in methanol extract of green jackfruit flour.

Sl. No.	Name	Ret. Time	Area	Height	Concentration ($\mu\text{g}/\text{mg}$)
1	Ascorbic acid	4.223	294,491	35,608	17.29
2	Gallic acid	5.712	96,769	16,767	5.69
3	Catechin	11.520	73,497	7891	4.32
4	Methyl gallate	12.436	30,776	3117	1.81
5	Caffeic acid	14.586	21,652	2539	1.27
6	Syringic acid	15.033	14,842	2119	0.87
7	Rutin	18.396	11,618	1976	0.68
8	p-Coumaric acid	19.068	15,034	2077	0.88
9	Sinapic acid	19.851	38,537	6079	2.26
10	Ferulic acid	20.996	55,995	6370	3.29
11	Myricetin	23.226	17,352	2102	1.02
12	Quercetin	28.368	11,515	1267	0.68
13	Apigenin	32.265	96,531	8183	5.67
14	Kaempferol	34.993	107,714	10,321	6.32

3.2. Effect of Isolated Fractions on Multiple Diabetic Enzyme Inhibition

Table 1 shows the inhibitory activity of isolated fractions derived from methanol extraction of green jackfruit flour on AG, AM, and AR. Rutin isolated from methanol extract inhibited all the enzymes (IC_{50} : 22.00 $\mu\text{g}/\text{mL}$ (AM); IC_{50} : 7.86 $\mu\text{g}/\text{mL}$ (AG); IC_{50} : 2.75 $\mu\text{g}/\text{mL}$ (AR) more effectively than all other isolated fractions. Under the same conditions, acarbose and quercetin exhibited IC_{50} values of 29.00 $\mu\text{g}/\text{mL}$ (AM), 11.05 $\mu\text{g}/\text{mL}$ (AG), and 4.00 $\mu\text{g}/\text{mL}$ (AR), respectively, indicating that MJ and its isolated fractions had a stronger inhibitory impact in this experiment. Rutin and all isolated fractions demonstrated considerably higher ($p \leq 0.05$) IC_{50} values than acarbose and quercetin on yeast AG, AM, and AR.

3.3. Enzyme Kinetics of Multiple Diabetic Enzyme Inhibition by Rutin

To elucidate the manner of AM, AG, and AR inhibition, kinetic analysis was performed for rutin by incubating with different doses of starch (0.5–8%), pNPG (4-Nitrophenyl- β -D-glucopyranoside) (0.25–4 mmol L^{-1}), and DL-glyceraldehyde (2.5–40 mmol L^{-1}), respectively, in the absence (control) or presence of rutin at IC_{20} , IC_{40} , and IC_{60} inhibitory concentrations ($\mu\text{g}/\text{mL}$). Lineweaver–Burk (LB) plots in the reaction were used to determine the mode of inhibition, K_m , and V_{max} values. Figure 1A–C illustrate LB plots of rutin against the inhibition of AM, AG, and AR, respectively. The results show that rutin caused a decrease in V_{max} values compared to the control, with a corresponding increase in K_m value (without substantial change in K_m values), which is typical of reversible, mixed-type plots. Competitive and non-competitive inhibition are combined in mixed-type inhibition. The kinetic manner of inhibition of starch, pNPG, and DL-glyceraldehyde by rutin was mixed, with increasing concentrations resulting in a succession of lines on the y-axis with the same intercept but various gradients. Rutin exhibited a mixed-type of inhibition against all the enzymes tested viz. AM (K_1 : 8.80 $\mu\text{g}/\text{mL}$; K_2 : 12.34 $\mu\text{g}/\text{mL}$), AG (K_1 : 11.50 $\mu\text{g}/\text{mL}$; K_2 : 15.15 $\mu\text{g}/\text{mL}$), and AR (K_1 : 37.86 $\mu\text{g}/\text{mL}$; K_2 : 59.05 $\mu\text{g}/\text{mL}$). K_1 and K_2 are two types of inhibitor constants used in mixed inhibition. The kinetics of rutin inhibition against all the enzymes revealed that K_2 values of rutin were greater than K_1 , indicating that rutin has a stronger affinity for free enzymes than for enzyme–substrate complexes.

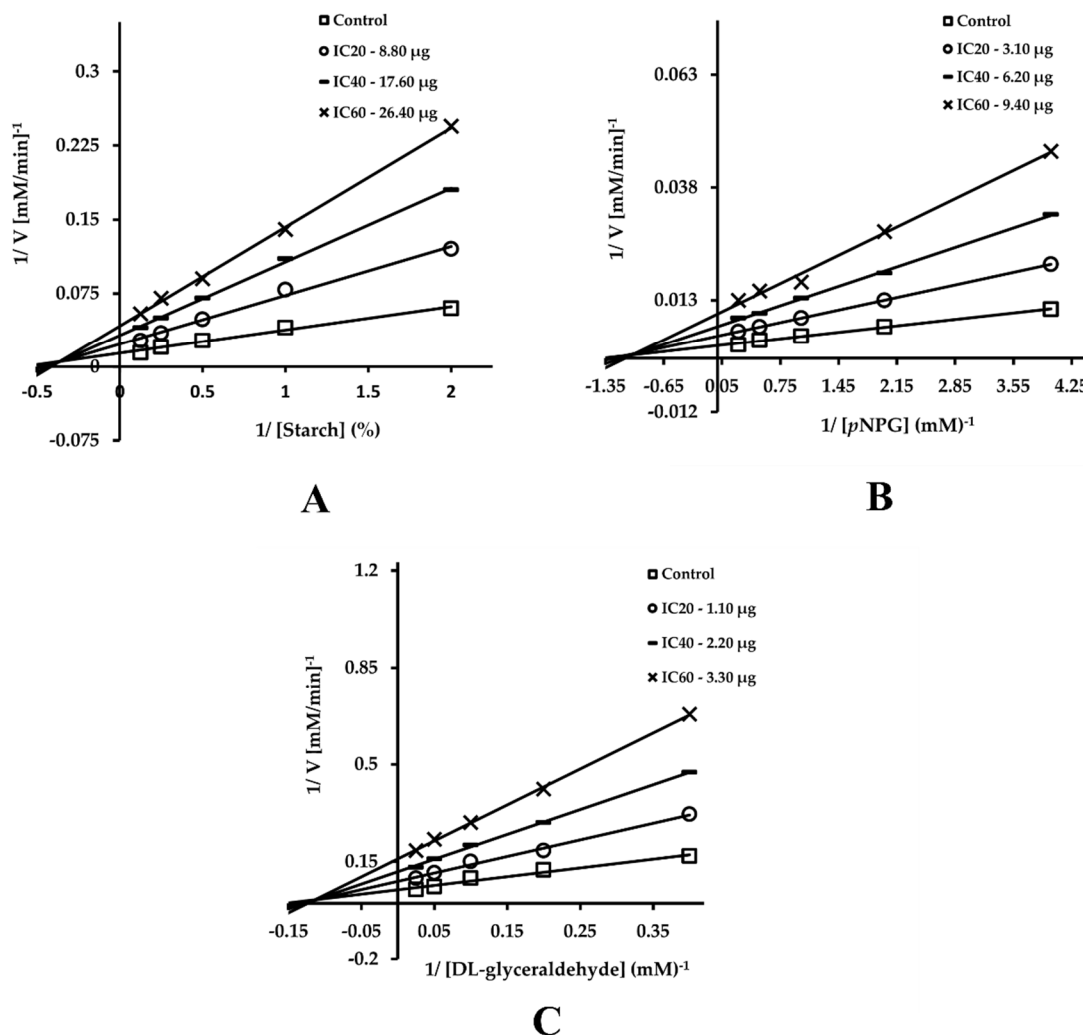


Figure 1. Rutin inhibitory potential of α -amylase (A), α -glucosidase (B), and aldose reductase (C) via Lineweaver–Burk plot of substrate-dependent enzyme kinetics. A-amylase, α -glucosidase, and aldose reductase were incubated with different doses of starch (0.5–8%), *p*NPG (0.25–4 mmol L⁻¹), and DL-glyceraldehyde (2.5–40 mmol L⁻¹), respectively, in the absence (control) or presence of rutin at IC₂₀, IC₄₀, and IC₆₀ inhibitory concentrations (μ g mL⁻¹).

3.4. Antioxidant Activities of the Isolated Fractions

DPPH, ABTS, and superoxide radical scavenging assay methodologies were used to assess the antioxidant properties of the separated MJ fractions (Table 1). In all parameters, rutin had stronger antioxidant activity than BHA (positive control). Additionally, in comparison to the positive control, all fractions examined had better radical scavenging properties (Table 1). The antioxidant activity of the investigated samples, as determined by DPPH, ABTS, and the superoxide radical scavenging method, might be ordered as follows: Rutin > MJ > ethyl acetate fractions > BHA in terms of EC₅₀ values.

3.5. Antiglycation Potential of Rutin

In the antiglycation assay, HSA comprising fructose, rutin, or aminoguanidine (positive control) at varying concentrations was utilized. In sterile circumstances, the reaction mixture was incubated at 37 °C for 21 days. After 21 days, it was clear that rutin had strong inhibitory actions (at all stages) compared with the positive control with various concentrations. Rutin (88%) and aminoguanidine (68%) were found to suppress the synthesis of fructosamines at a concentration of 100 μ g/mL, whilst protein carbonyl com-

pounds were inhibited at 91% and 70%, respectively. Rutin and aminoguanidine have been shown to reduce the production of AGE by 51% and 74%, respectively. In the presence of rutin, thiol shielding values were found to be 82% (concentration 100 µg/mL). Under the same assay conditions, aminoguanidine (concentration 100 µg/mL) exhibited 75% thiol group protection.

3.6. Molecular Docking Simulation

Molecular docking simulation results show that rutin had the higher (most negative) binding affinity among all the ten phenolic compounds screened for the four target proteins, whereas the controls had a lesser binding affinity. The virtual screening of the compounds based on the binding affinity and the total number of bonds formed is detailed in Table 3. While interacting with AG, rutin also formed the highest non-bonding interactions (thirteen); nine turned out to be hydrogen bonds. The hydrogen bonds formed by rutin included ARG 439 (2.71 Å), ASP 349 (2.18 Å and 2.17 Å), HIS 279 (2.95 Å), GLU 276 (2.63 Å), THR 307 (2.29 Å), ARG 312 (3.15 Å), PHE 157 (1.85 Å), and HIS 245 (2.97 Å). Two hydrophobic interactions, including a pi–pi stacked bond with HIS 279 (5.53 Å), and a pi–sigma bond with PRO 309 (2.46 Å) were formed. There were two electrostatic pi-anion bonds formed with GLU 304 (4.17 Å and 3.72 Å). With all these binding interactions, rutin had a binding affinity of −10.5 kcal/mol, whereas acarbose was found to have only seven non-bonding interactions with all of them being hydrogen bonds. These include GLU 304 (2.36 Å), SER 308 (1.92 Å), HIS 279 (2.49 Å), THR 307 (2.55 Å), PHE 157 (3.56 Å), HIS 239 (3.02 Å), and PRO 309 (1.77 Å). With these binding interactions, acarbose was predicted with −8.2 kcal/mol binding affinity. The binding interactions of rutin and acarbose with AG are visualized in Figure 2. In the case of AM, rutin bound with the key residue was involved with the catalytic mechanism, GLU 233 with two hydrogen bonds (2.85 Å and 2.16 Å). In total, rutin was predicted with ten non-bonding interactions, in which seven of them were found to be hydrogen bonds. Apart from GLU 233, it formed five hydrogen bonds with HIS 101 (2.42 Å), HIS 299 (2.94 Å), ARG 195 (2.11 Å), TYR 151 (1.93 Å), and HIS 201 (2.04 Å). It also formed hydrophobic pi–pi bonds with TRP 59 (5.13 Å and 4.53 Å) and TYR 62 (4.65 Å). With these interactions, rutin had a binding affinity of −10.2 kcal/mol. While binding with AM, acarbose interacted with the GLU 233 with a single hydrogen bond (2.40 Å). However, apart from this, it was predicted with only four hydrogen bonds with HIS 101 (2.71 Å), TRP 59 (2.68 Å), ASP 300 (2.78 Å), and ASN 298 (2.75 Å). Acarbose did not form any hydrophobic or electrostatic bonds, and it had a binding affinity of −8.9 kcal/mol. The binding interactions of rutin and acarbose with AM are visualized in Figure 3. Both rutin and aminoguanidine are bound with the same binding site in the case of HSA, which is located at the subdomain IIIA, bound with co-crystallized ligand ibuprofen. Rutin formed a total of fourteen non-bonding interactions, where six of them were found to be hydrogen bonds. In the subdomain IIIA, rutin was predicted to bind with the key residues such as ASN 489 (2.39 Å), ARG 410 (2.19 Å), TYR 411 (2.57 Å), and VAL 433 (2.55 Å) with hydrogen bonds. Two hydrophobic pi–alkyl bonds were formed with VAL 433 (4.64 Å) and LEU 430 (5.44 Å). In addition, rutin formed a pi–sigma bond with LEU 453 (4.61 Å). Apart from these interactions, rutin bound with ASN 391 with two hydrogen bonds (1.87 Å and 3.26 Å), CYS 438 (4.94 Å) with a pi–sulfur bond, and ALA 449 (4.66 Å) with a pi–alkyl bond. With these interactions, rutin had a binding affinity of −9.9 kcal/mol. However, aminoguanidine was not able to bind properly with HSA. It had formed only two hydrogen bonds with ARG 485 (2.93 Å and 2.86 Å). There were two unfavorable bonds present, LYS 414 (3.04 Å and TYR 411 Å). With these bonds, aminoguanidine had a binding affinity of −6.4 kcal/mol. The visualization of binding interactions of rutin and aminoguanidine with HSA is given in Figure 4. In addition, both rutin and quercetin occupied the same binding site of the co-crystallized ligand zenarestat, which is located near to the NADPH binding site. Rutin formed a total of ten non-bonding interactions with HAR, including six hydrogen bonds. The hydrogen bonds included TYR 48 (1.81 Å), TRP 111 (1.78 Å), TRP 20 (2.52 Å), VAL 47 (2.93 Å), GLN 49 (2.45 Å), and PHE 122 (2.14 Å). It also formed three pi–alkyl bonds

with CYS 298 (3.58 Å), TRP 219 (4.98 Å), and PRO 218 (5.48 Å). Altogether, rutin’s binding affinity was −10.2 kcal/mol with these interactions, whereas quercetin formed a total of eight non-bonding interactions, which included a single hydrogen bond. It is bound with TRP 20 (5.03 Å) and TRP 111 (5.74 Å and 5.22 Å) with hydrophobic pi–pi bonds. It is also bound with LEU 300 with (5.13 Å and 3.63 Å). However, two unfavorable bonds with CYS 298 (2.39 Å) and TYR 309 (2.42 Å) were also present. With these interactions, quercetin was found with a binding affinity of −7.8 kcal/mol. The visualization of binding interactions of rutin and quercetin with HAR is depicted in Figure 5.

Table 3. Binding affinity, total number of non-bonding interactions, and hydrogen bonds formed by phenolic compounds during docking simulation.

Sl. No.	Name of the Compound	α-Glucosidase			α-Amylase			HSA			HAR		
		BA	NB	HB	BA	NB	HB	BA	NB	HB	BA	NB	HB
1	Ascorbic acid	−5.2	3	2	−7.5	7	2	−8.1	8	2	−6.2	5	1
2	Gallic acid	−6.4	3	2	−8.2	8	1	−7.7	7	2	−7.8	6	0
3	Catechin	−6.4	2	1	−9.1	5	2	−7.1	6	2	−8.3	8	2
4	Methyl gallate	−8.2	5	4	−8.1	6	3	−6.4	9	3	−7.2	4	3
5	Caffeic acid	−5.9	8	5	−6.2	5	1	−7.0	8	4	−8.2	7	1
6	Syringic acid	−8.4	11	6	−9.1	9	4	−8.9	10	5	−9.0	8	4
7	Rutin	−10.5	13	9	−10.2	10	7	−9.9	14	6	−10.2	10	6
8	p-Coumaric acid	−5.8	7	5	−8.3	9	6	−9.1	7	1	−9.7	9	3
9	Sinapic acid	−5.6	8	4	−7.2	7	3	−8.4	8	2	−8.2	5	2
10	Ferulic acid	−8.0	6	5	−6.5	8	3	−7.1	8	2	−6.2	8	3
11	Myricetin	−9.1	5	5	−8.9	5	2	−9.2	7	4	−7.8	6	5
12	Apigenin	−8.1	6	2	−7.2	8	2	−8.1	5	2	−8.6	5	2
13	Kaempferol	−8.5	7	3	−8.0	7	5	−7.4	6	3	−9.1	7	6
14	Acarbose	−8.2	7	7	−8.9	5	5	-	-	-	-	-	-
15	Amino-guanidine	-	-	-	-	-	-	−6.4	2	2	-	-	-
16	Quercetin	-	-	-	-	-	-	-	-	-	−7.8	8	1

Note: BA: binding affinity in kcal/mol, NB: Total number of non-bonding interactions, HB: Total number of hydrogen bonds, HSA: human serum albumin, HAR: human aldose reductase.

3.7. Molecular Dynamics Simulation

Since rutin had the highest number of interactions and the most negative binding affinity, it was selected for simulation. Based on the results obtained from the simulations that were run for 100 ns, trajectories were plotted in terms of RMSD, RMSF, Rg, SASA, and ligand hydrogen bonds. The stability of the protein–ligand complexes is depicted in the RMSD plot of the simulation. The Rg plot plots illustrate the structural compactness of the molecules by calculating their RMSD with respect to the central axis of rotation. The RMSF plots show a particle’s average deviation from a reference point over time. It examines the regions of the protein–ligand complex or protein backbone structure that differ the most/least from the mean. Furthermore, the area around the hydrophobic core created between protein–ligand complexes is shown in the SASA plots. Since few hydrogen bonds were concurrently disrupted and rebuilt, it is critical to calculate the number of hydrogen bonds produced during the simulation.

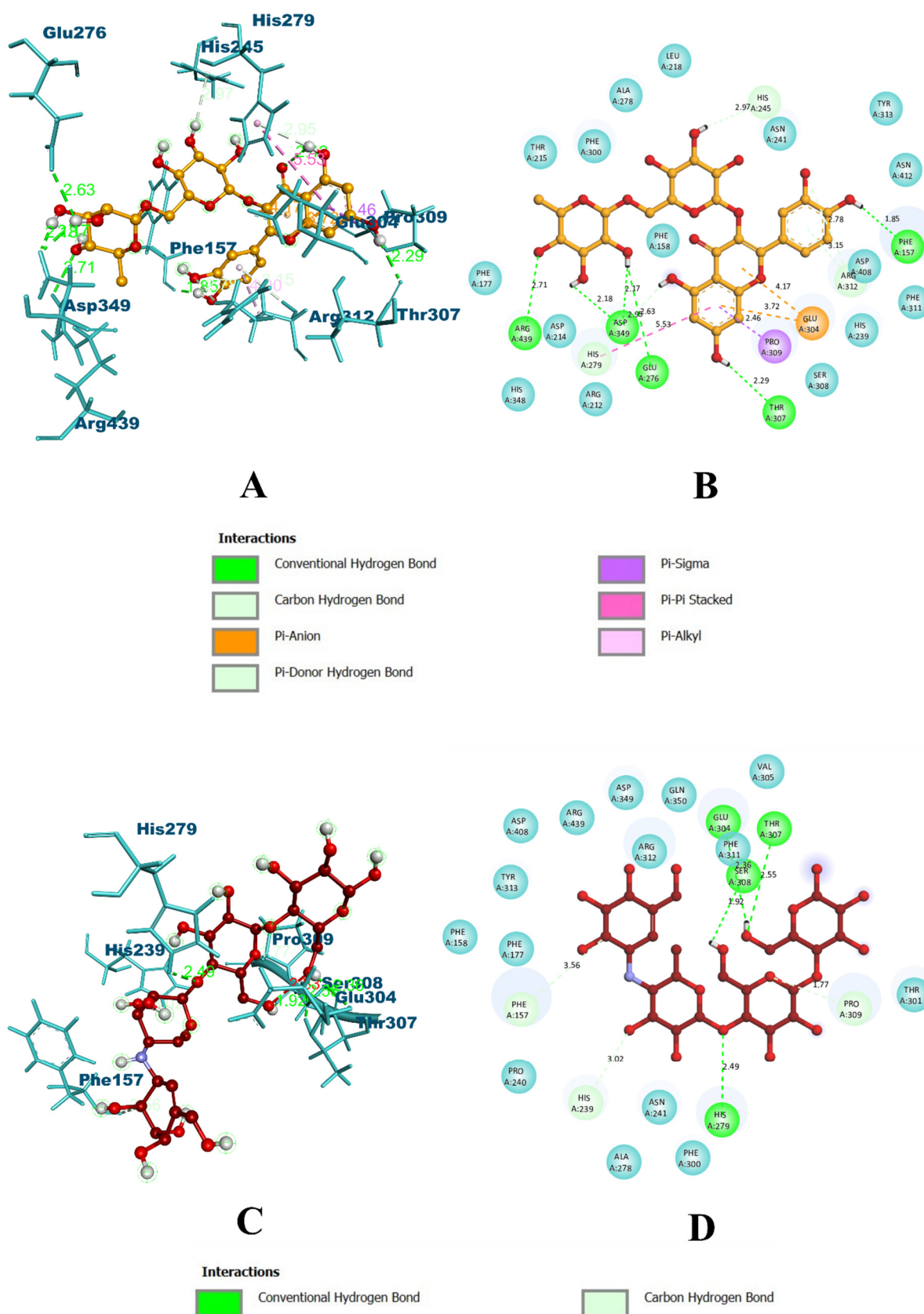


Figure 2. Visualization of docking simulation of experimental compounds with α -glucosidase. (A,B) Interaction of rutin acid visualized in 3D and 2D; (C,D) Interaction of acarbose visualized in 3D and 2D, respectively. Colored: bound residues, turquoise blue: surrounding residues.

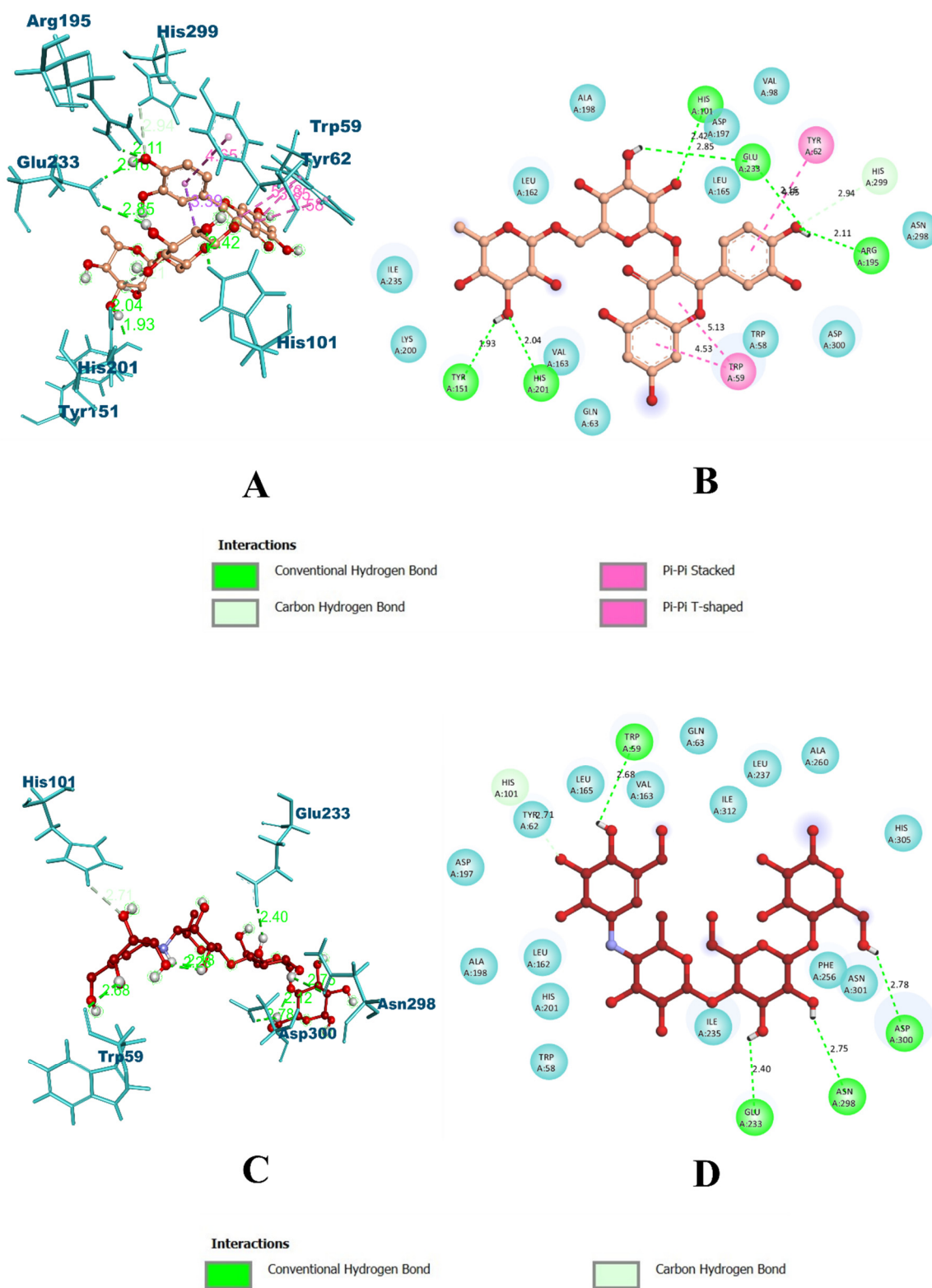


Figure 3. Visualization of docking simulation of experimental compounds with α -amylase. (A,B) Interaction of rutin visualized in 3D and 2D; (C,D) Interaction of acarbose visualized in 3D and 2D, respectively. Colored: bound residues, turquoise blue: surrounding residues.

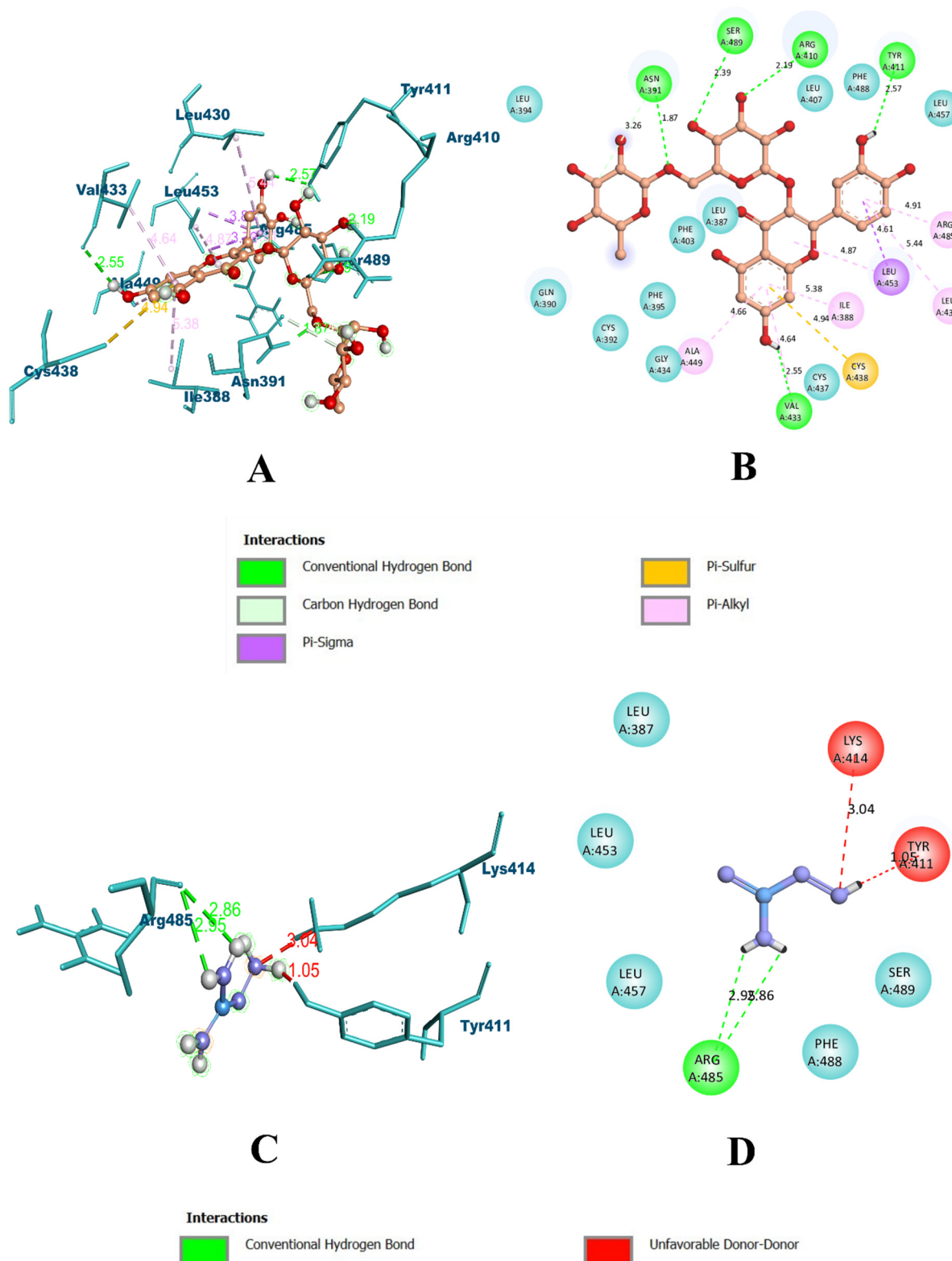


Figure 4. Visualization of docking simulation of experimental compounds with HSA. (A,B) Interaction of rutin visualized in 3D and 2D; (C,D) Interaction of aminoguanidine visualized in 3D and 2D, respectively. Colored: bound residues, turquoise blue: surrounding residues.

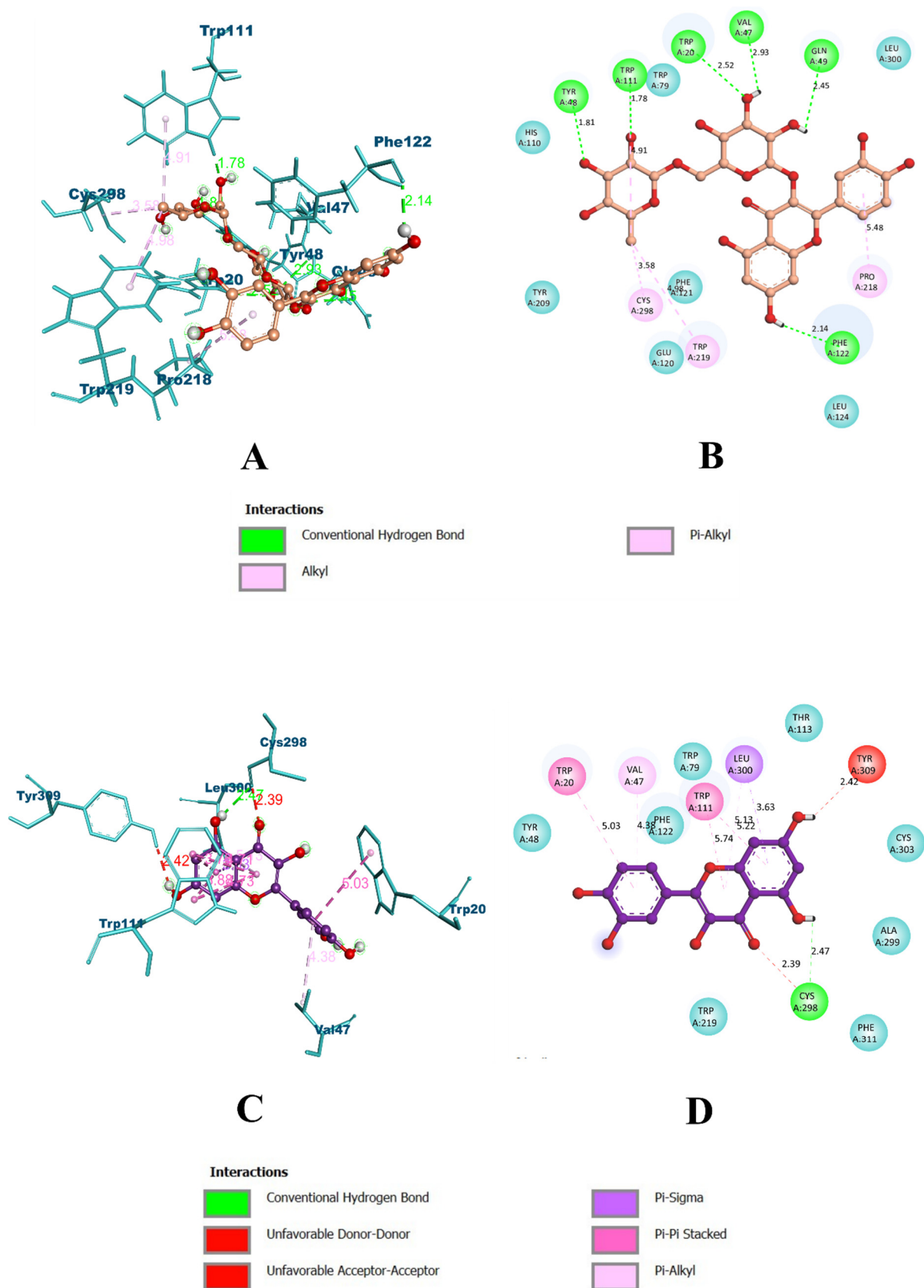


Figure 5. Visualization of docking simulation of experimental compounds with HAR. (A,B) Interaction of rutin visualized in 3D and 2D; (C,D) Interaction of quercetin visualized in 3D and 2D, respectively. Colored: bound residues, turquoise blue: surrounding residues.

The simulation trajectories obtained for AG complexed with rutin and acarbose revealed that all the RMSD plots become stabilized after 20 ns, reaching equilibrium after initial fluctuations. The RMSD value of bare protein atoms and the protein–rutin complex was found to range between ~0.35 and 0.40 nm. On the other hand, the RMSD of the protein–acarbose complex was found to be between ~0.30 and 0.35 nm. In the case of bare protein atoms, Rg value was found to be ~3.3 nm, whereas both protein–rutin and protein–acarbose showed the Rg value ranging between ~2.3 and 2.4 nm. In the case of RMSF analysis, bare protein atoms were predicted with fluctuations at terminal and loop regions. However, the protein–acarbose complex showed higher fluctuations than the protein–rutin complex (200–300 and 400–500 residues). Further, in the case of bare protein atoms, the SASA value was found to range between 350 and 375 nm². Both protein–rutin and protein–acarbose showed similar patterns, with the SASA value of 225 nm². In the case of ligand hydrogen bonds, rutin formed a maximum number of nine bonds, whereas acarbose was able to form only five of them. This indicates the stronger binding affinity and stability of rutin with the protein compared to acarbose. Even though similar patterns were observed in case of RMSF, SASA, and Rg, rutin poses a better ligand in comparison with acarbose during other trajectory analyses. Results from molecular dynamics simulation reveal rutin as a stable and stronger inhibitor of AG in comparison with acarbose. The visualization of simulation results for AG is summed up in Figure 6A1–A4.

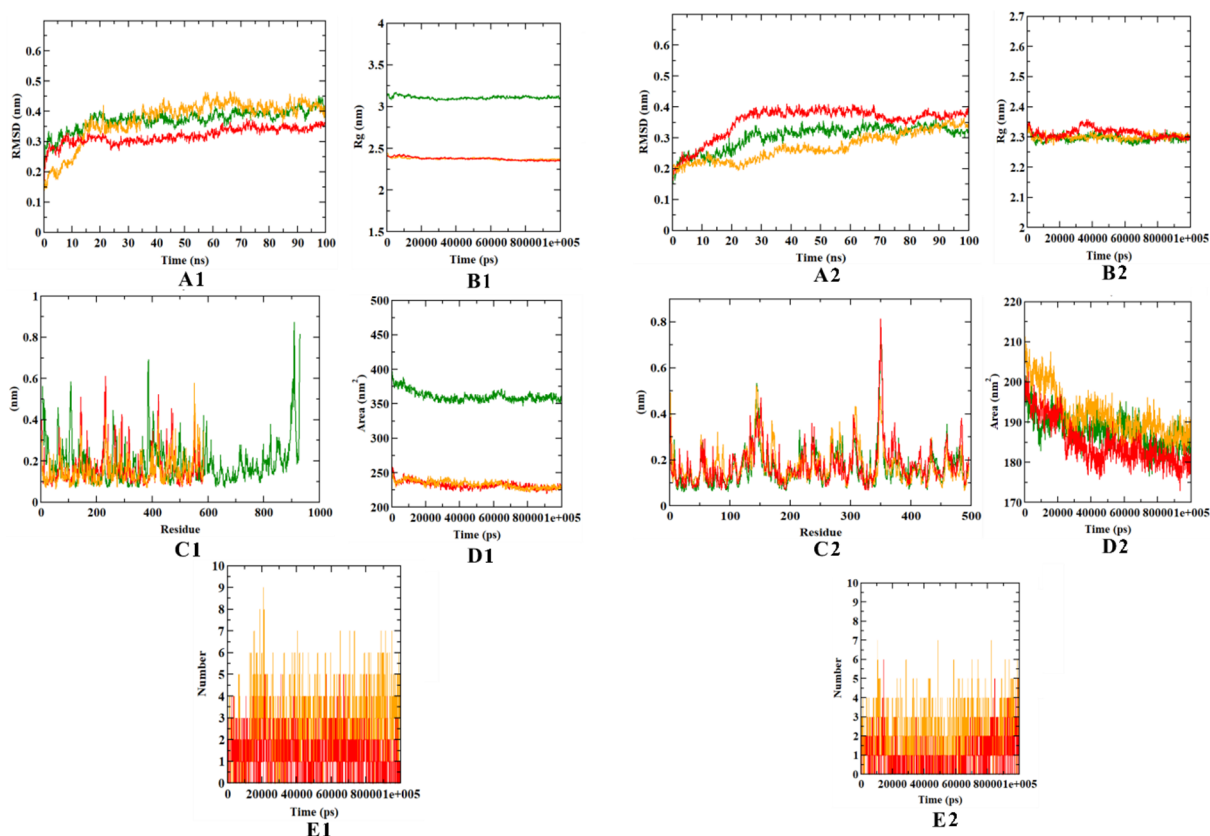


Figure 6. Cont.

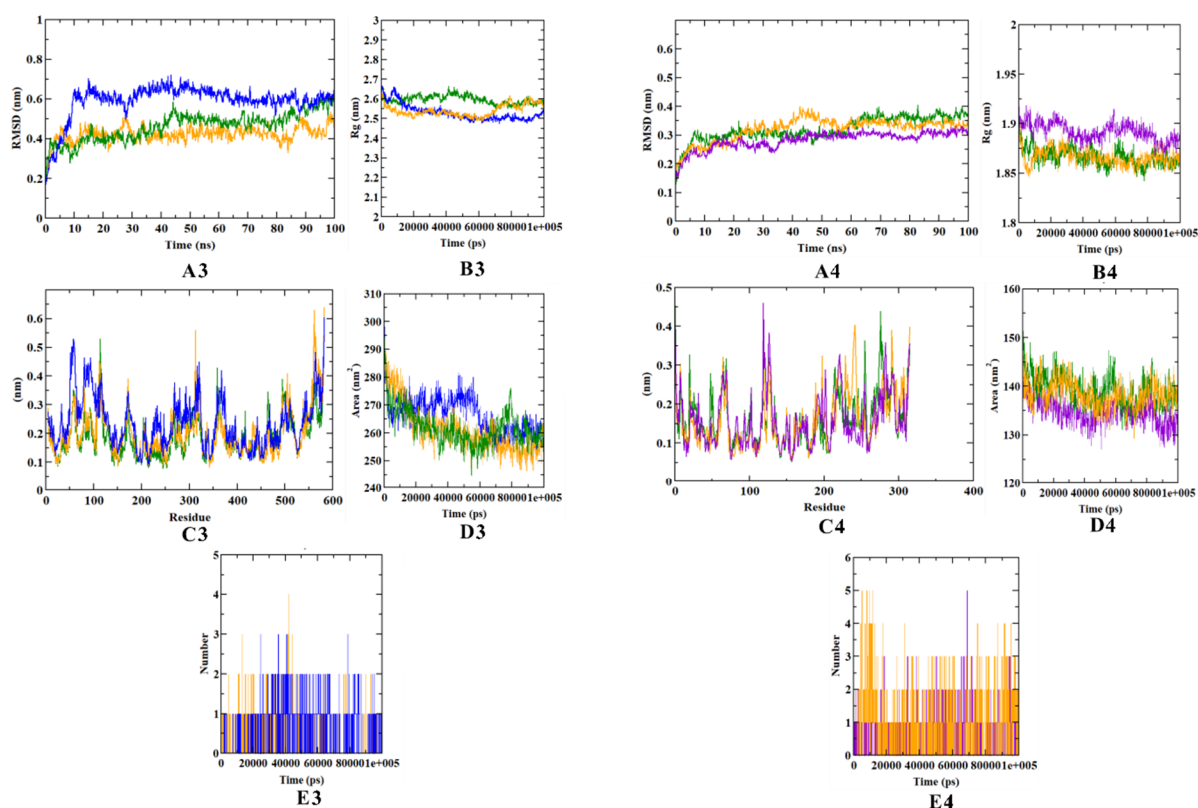


Figure 6. Visualization of trajectories obtained from molecular dynamics simulation. (A1–A4): RMSDs of proteins and protein–ligand complexes for α -glucosidase, α -amylase, HSA, and HAR, respectively. (B1–B4): Rg, (C1–C4): RMSF, (D1–D4): SASA, and (E1–E4): ligand hydrogen bonds. Green: protein backbone atoms, orange: protein–rutin complex, red: protein–acarbose complex, blue: protein–aminoguanidine complex, violet: protein–quercetin complex.

In the case of AM, the RMSD plots reveal that protein backbone and protein–acarbose complex becomes stabilized at 30 ns, whereas the protein–rutin complex becomes stabilized at 35 ns. However, both bare protein atoms and protein–rutin complexes become equilibrated at between 0.3 and 0.35 ns, and the protein–acarbose complex becomes equilibrated at between 0.35 and 0.40 ns. Meanwhile, the RMSD plots of the protein backbone and protein–acarbose complex are not found to be as concurrent as that of the protein–rutin RMSD plot. The Rg plots also depict the same pattern, where all the plots equilibrate at 2.3 nm. However, plots of the protein–rutin complex and bare protein atoms are more concurrent with each other. The RMSF plots depict the comparative instability of the protein–acarbose complex, where the fluctuations at loop regions (about 350th residue) were found to be higher (0.8 nm) than that of the protein–rutin complex plots (0.45 nm). The SASA plots reveal that both protein backbone atoms and protein–rutin complex become equilibrated at between 185 and 190 nm², whereas the protein–acarbose complex becomes equilibrated at 180 nm². This brings interference in the concurrency between the plots of bare protein atoms and the protein–acarbose complex. Further, acarbose was predicted to form five hydrogen atoms during MD simulation, whereas rutin was found with seven of them. Results from these simulations depict that rutin had comparatively higher stability than acarbose. The visualization of MD trajectories of AM complexed with experimental molecules is given in Figure 6B1–B4. During the analysis of MD simulation results of HSA with rutin and aminoguanidine, it was found that the RMSD of plots of both bare protein atoms become stabilized after 15 ns. Moreover, the protein–aminoguanidine complex becomes stabilized after 40 ns. The concurrency between the RMSD plots of protein backbone atoms and protein–rutin complexes was found to be higher in comparison with that of the protein–acarbose complex and bare protein atoms. The Rg plots also reveal the structural

compactness of the protein–rutin complex over the protein–aminoguanidine complex, where both bare protein atoms and protein–rutin complexes become equilibrated at 2.6 nm and the protein–aminoguanidine complex at between 2.5 and 2.6 nm. The RMSF plots show that the protein–aminoguanidine complex had higher fluctuations in comparison with that of the protein–rutin complex throughout the simulation run. However, protein–rutin was found with fluctuations only in the loop regions (about 300th residue) and c-terminal regions. In the case of the SASA plots, all the plots become equilibrated at between 250 and 265 nm². However, the SASA plot of the protein–aminoguanidine complex was not in concurrence with that of the bare protein atoms. Further, aminoguanidine formed only three hydrogen bonds at the maximum during the simulation, whereas rutin formed four of them during the same. Figure 6C1–C4 detail the visualization of the MD trajectories obtained for the HSA complexed with rutin and aminoguanidine. In the case of HAR, the RMSD plots of bare protein atoms, protein–rutin complex, and protein–quercetin complex became stabilized after the initial fluctuation at 5 ns. All the plots become equilibrated in the range from 0.3–0.4 nm. However, the RMSD plot of the protein–rutin complex appears to have more concurrency with that of the bare protein atoms, in comparison with the protein–quercetin plot. The Rg plots also depict the same pattern, where bare protein atoms and the protein–rutin complex equilibrate at between 1.85 and 1.875 nm, whereas the protein–quercetin complex equilibrates at between 1.875 and 1.90 nm. In the case of RMSF plots, the protein–quercetin plot shows more fluctuations at loop regions (100–150 residues, 200–250 residues), in comparison with the protein–rutin complex. However, at terminal regions, fluctuations of the protein–rutin complex were found to be high. Moreover, the protein–rutin complex was predicted with minimal fluctuations throughout the simulation. The same pattern was continued with the SASA plots, where bare protein atoms and protein–rutin complexes were predicted with the SASA value of between 135 and 140 nm², yet the protein–quercetin complex was found with the SASA value of between 130 and 135 nm². In the case of ligand hydrogen bonds, both quercetin and rutin were able to form an equal number of hydrogen bonds (five) during the course of MD simulation. Visualization of MD trajectories obtained for HAR complexed with rutin and quercetin is depicted in Figure 6D1–D4.

3.8. Binding Free Energy Calculations

The extent of binding is represented by the binding free energy of ligands bound to protein structures. Binding free energy is released during the creation of a protein–ligand complex and is used to determine whether or not the complex is stable. The creation of a stable complex is better described by binding free energy with a lower value. Van der Waal's, electrostatic, polar solvation, SASA, and binding energy were used to calculate the binding free energy in this case. In this experiment, the AG–rutin complex (−324.712 kJ/mol) showed the highest binding free energy in comparison with all the other complexes. It significantly used van der Waal's force to form. In comparison with the other binding free energies, van der Waal's was found to be the major contributor to the protein–ligand complexes. In addition, all the protein–rutin complexes were found to have higher (more negative) binding free energies in comparison with all the protein–control drug complexes. Results from binding free energy calculations support the results obtained from MD simulations in terms of stability and binding efficiency. Types of binding free energies and standard deviations of all protein–ligand complexes have been summarized in Table 4.

Table 4. Binding free energy calculations of target proteins complexed with experimental ligands.

Protein-Ligand Complexes	Values and Standard Deviations	Types of Binding Free Energies				
		Van der Waal's Energy (kJ/mol)	Electrostatic Energy (kJ/mol)	Polar Solvation Energy (kJ/mol)	SASA Energy (kJ/mol)	Binding Energy (kJ/mol)
α-glucosidase-rutin	EV	−324.712	−5.382	92.618	−24.746	−260.222
	SD	±21.580	±4.082	±13.384	±1.441	±21.396
α-glucosidase-acarbose	EV	−134.192	−4.813	62.125	−9.310	−90.102
	SD	±180.341	±9.475	±58.801	±14.719	±145.076
α-amylase-rutin	EV	−204.258	−2.931	42.572	−16.289	−180.906
	SD	±117.430	±4.057	±39.446	±9.495	±118.715
α-amylase-acarbose	EV	−130.161	−2.106	39.340	−9.564	−87.109
	SD	±100.269	±22.186	±54.310	±6.998	±61.672
HSA-rutin	EV	−161.503	−5.499	55.663	−9.513	−99.851
	SD	±41.895	±6.908	±34.324	±3.103	±22.691
HSA-aminoguanidine	EV	−150.719	−5.127	47.498	−7.981	−81.872
	SD	±99.469	±10.298	±57.619	±8.124	±79.501
HAR-rutin	EV	−184.694	−6.705	97.407	−9.678	−93.670
	SD	±81.018	±6.141	±30.480	±7.049	±70.236
HAR-quercetin	EV	−171.669	−3.291	81.102	−8.781	−85.768
	SD	±110.361	±34.678	±79.539	±15.786	±92.766

Note: EV: Energy values, SD: standard deviation, HSA: human serum albumin, HAR: human aldose reductase.

4. Discussion

Successful hyperglycemia intervention is critical for reducing the frequency, progression, and severity of diabetes complications. On the other hand, using a single therapy technique has not been successful in preventing all of the negative consequences of high blood glucose levels [39]. As a result, AG inhibitors, AR inhibitors, antiglycation medications, and antioxidants may be viable choices for lowering the negative impact exerted by persistent circulating glucose. Numerous studies have demonstrated that basic plant extract as well as bioactive combinations produced from it can aid in the reduction of blood glucose levels [40,41]. Enumerable studies have shown that the unrefined plant concentrate, as well as its bioactive molecules present in these extracts, are effective in lowering blood glucose levels. In this regard, several bioactive ingredients isolated from plants have been identified for their potential glucose-lowering abilities [41]. Rutin is one such plant flavonoid that has anti-diabetic activity induced via reducing the expression of insulin-resistant molecules, enabling the interaction between insulin and its receptors, inducing adipose tissue peroxisome proliferator-activated receptor (PPAR) expression and adipocyte-derived protein production, according to studies through molecular and physiological mechanisms [42]. Chen et al. (2020) demonstrated in an animal study that rutin-containing formulations significantly improved serum insulin and C-peptide concentrations, hexokinase, hyperlipidemia, liver glycogen content, hyperglycemia, glucose-6-phosphatase, and glycogen phosphorylase activities in type 2 diabetes mellitus (DM) rats that were orally treated with rutin [43]. Rutin caused a significant improvement in peripheral glucose levels in rat diaphragm studies. It has demonstrated potent antioxidant properties observed by its lowering abilities on lipid peroxidation and the generation of thiobarbutiric acid reactive species (TBARS).

The metabolic process in the body is initiated by the conversion of dietary glucose into energy, which is utilized primarily by AM and AG [44]. In the present study, rutin extracted from jackfruit flour was discovered to be a potent AG and AM inhibitor. An LB plot obtained from the kinetics data to explore the mechanism underlying this inhibition demonstrated a reversible, mixed pattern of inhibition. Mixed-type inhibition is a cross between competitive and non-competitive inhibition, with two different types of equilibrium constants, K1 and K2. The higher the inhibition, the lower the equilibrium constant.

The inhibition constants (K_1 and K_2) were found to have lower values in this study, and K_1 values were always smaller than K_2 values. From the study, it was revealed that rutin inhibits both AM and glucosidase, which is in line with earlier research [45]. The mixed form of inhibition was previously observed in flavonoids with comparable results [46].

When diabetes persists, excessive free glucose units cause a number of secondary problems, which must be considered while developing an optimal anti-diabetic treatment. In addition, the polyol pathway, which is a part of the intermediate metabolism, is harmed when glucose levels are too high [47]. According to studies, roughly 3% of glucose is metabolized through this route in normoglycemic situations, whereas glucose consumption increases to more than 30% in hyperglycemic states [48]. The AR catalyzes the conversion of glucose to sorbitol and serves as the pathway's rate-limiting step. Despite evidence that AR has a role in the detoxification of aldehydes, a by-product of lipid peroxidation, its role in carbohydrate metabolism is unknown. However, its inhibition has been known to prevent the development of diabetic retinopathy, which constitutes one of the serious complications of diabetes [49]. In the present study, rutin showed to be a potent AR inhibitor faring better than the reference standard quercetin. The LB plot demonstrated that the compound inhibited AR in a mixed-type manner. Flavonoids have been reported to alter carbohydrate digestion, insulin generation, insulin signaling, and glucose absorption in insulin-sensitive organs via interacting with several intracellular signaling pathways [50]. The link between flavonoid structure and AR inhibitory function has been discovered through various studies on flavonoid structure. In agreement with these studies, rutin also demonstrated an inhibitory effect of AR, and, in turn, exerting its effect on the polyol pathway.

Protein glycation is considered to possess some of the serious complications of diabetes [51]. Glycation of various proteins occurs when there is too much glucose in the bloodstream, rendering them inactive. Fructose has recently been discovered in glycation, either directly or through promoting fructose formation from glucose by activating the polyol pathway [7]. Fructose participates in glycation at a quicker pace than glucose, meaning greater adverse effects. The nucleophilic addition reaction between the free amino group of proteins and the carbonyl group of the reducing sugar initiates the creation of a Schiff's base, which results in irreversible Amadori products, such as fructosamines [7,20]. In the second stage of glycation, fructosamines are converted to a range of carbonyl compounds, including deoxyglucosones glyoxal and methylglyoxals, resulting in the formation of carbonyl proteins. The progression of this condition results in the formation of protein thiols. Overall, the progressive glycation process results in the formation of advanced glycation end products (AGE), the insoluble luminous products that bind to glycated proteins and accumulate in cells. They hinder normal protein function within the cells and create irregular cross-linking of the extracellular matrix, preventing it from performing its normal function [20]. Aside from causing vascular problems, AGEs also cause the development of reactive oxygen species (ROS), which has been related to the majority of diabetes problems [20,52].

With this background, in the present study, the initial stage of protein glycation was performed under *in vitro* conditions by exposing HSA to high fructose concentrations, which was expected to glycate HSA. Fructosamine levels were higher than non-glycated HSA levels in our study, as expected, and rutin therapy significantly reduced this, exceeding the standard inhibitor aminoguanidine [7,20]. The increased protein carbonyl groups generated after the exposure to a high fructose load, as well as the similarly low levels of protein thiols, demonstrated the second stage of protein glycation. Treatment with rutin reduced this to approximately 82%, showing that it has a protective effect. Finally, the compounds' ability to create fluorescent products was employed to measure AGE development in this study; the results revealed that AGE formation was significantly reduced [7,20]. As a result, the potential role of rutin in avoiding each stage of protein glycation has been confirmed, indicating that they may be effective in reducing the different complications arising due to diabetes. Conversely, aminoguanidine, an anti-glycation experimental drug, was found to be less effective than the compound tested [20].

Plant extracts have been well-known for their potential antioxidant properties owing to the presence of several bioactive components [53]. In this regard, in the present study, the antioxidant potential of rutin was evaluated using some of the standard assays, namely DPPH, ABTS, and superoxide. Our findings proved that rutin had improved free radical scavenging activity in all of the tests employed in the study, showing that it has a protective role against free radical-mediated damage. Several researchers have proven the remarkable antioxidant potential of flavonoids present in plant extracts [54]. In all of the investigations, the extracts containing the greatest phenolic compounds and flavonoids were found to be the most powerful antioxidants, protecting against oxidative damage caused by free radicals in diseases such as cancer, diabetes, asthma, dementia, Parkinson's disease, and others [54]. In agreement with the previous studies, rutin showed noteworthy antioxidant ability in comparison with that of standard ascorbic acid.

Molecular docking simulations are used to determine the molecular interactions between ligands and target proteins; they determine the extent of ligand binding, which indicates whether or not a protein is inhibited or activated [55]. We chose rutin, a flavonoid found in jackfruit flour to target the inhibition of AG, AM, HSA, and HAR in this work. Rutin exhibited the highest binding affinity with all of the target proteins, according to the docking simulation results.

All experimental compounds were bound deep within the binding pocket during the docking simulation of AG. According to a previous study by Patil et al. (2021), the docking was accurate [28]. The interaction of rutin was found to be superior to that of acarbose, despite the fact that both the ligands were found docked inside the binding pocket. The binding affinity of rutin was high because the number of hydrophobic linkages (π - π and π -alkyl) was deemed higher than the number of hydrogen bonds [56]. In the case of AM, HSA, and HAR, rutin showed the same pattern. When compared to other non-bonding interactions, all four proteins bound with rutin employed more hydrophobic bonds. In all the four target proteins, control drugs were not able to form more hydrophobic bonds, and their binding efficiency was not up to the mark of rutin. The binding interaction analysis of compounds docked with AM shows that both rutin and acarbose were bound to the key residue GLU 233. However, due to the hydrophobic bonds and other non-bonding interactions, such as hydrogen bonds, rutin was found to have more binding affinity than acarbose. Binding to this catalytic residue (GLU 233) would effectively reduce the activity of AM, as indicated in recent studies [57,58]. Moreover, the binding of rutin to both the carbohydrate digestion enzymes was in accordance with a previous study conducted by Osman et al. (2021) [59] and Jhong et al. (2015) [60]; these studies used different sources of rutin, yet the docking results are similar.

In case of HSA, all the compounds were bound to binding site II, which is made of 6 helices of subdomain III. Binding site II consists of a polar patch, which consists of key residues ARG 410, TYR 411, SER 489 LEU 430, and LEU 453. These residues are present in the vicinity of fatty acid site 4 (FA4), which accommodates the methylene tails of lipids bound to this site [61]. Moreover, the ligands occupied the same binding site of the co-crystallized ligand ibuprofen. According to a study, binding into the polar patch of the binding pocket induces conformational changes in the protein [62]. As rutin was bound to these key residues of the polar patch of binding site II, it is expected to induce conformational changes in HSA. However, aminoguanidine was not able to bind to these residues. The docking results were in accordance with the study performed by Isogai and Hirayama (2013) [61] and Ali et al. (2022) [63]. While binding with HAR, both rutin and quercetin occupy the same binding site as the co-crystallized ligand zenarestat, which is present in the proximity of the NADPH binding site. The NADPH-dependent conversion of glucose to sorbitol, which is the initial step in the polyol pathway of glucose metabolism, is catalyzed by HAR [64].

We performed the MD simulations for all the protein–ligand complexes formed as a result of molecular docking. The overall stability of the protein–ligand combination kept in a particular environment for a specific period of time is assessed using molecular dynamics

simulation. Simulating experimental molecules with their target proteins has given variable results in this study.

In the case of AG, rutin acid is the most stable compound according to all graphs. In none of the plots was the protein–rutin acid complex predicted with aberrant variations (RMSD, RMSF, Rg, SASA, and ligand hydrogen bonds). Protein–acarbose complex plots, on the other hand, were not as similar as the protein–rutin complex with the bare protein atoms. The simulations of all four target proteins showed the same pattern in case of rutin. During the simulation study, the concurrent plots of the protein–ligand complex with the bare protein atoms show a greater binding affinity [65,66]. In the case of AM, protein–acarbose complex was found to be relatively unstable in comparison with the protein–rutin complex. Simulated plots of a protein–rutin acid complex were consistent with earlier research by Kumar et al. (2021) [67].

Further, dynamics simulation trajectory analysis of HSA complexed with caffeic acid and aminoguanidine showed similar patterns of instability compared with that of the protein–syringic acid complex. However, a study by Soltanabadi et al. (2018) depicted the binding stability of cinnamaldehyde [68]. Since the simulation was performed for only 20 ns, it was difficult to predict the overall stability of the protein–cinnamaldehyde complex. Moreover, our study clearly established the protein–syringic acid complex as the stable complex through 100 ns simulation. This result was in accordance with a study that evaluated the stability of the HSA–phycocyanobilin complex [69]. Furthermore, the relative instability of the protein–quercetin complex is depicted in the dynamics simulation results of HAR complexed with the experimental molecules. The protein–rutin complex has been considered stable in comparison with the protein–quercetin complex. The outcomes of the HAR simulation were consistent with a study that suggested kusunokinin as a potential HAR inhibitor [70].

We have also evaluated the binding free energy calculations using the MMPBSA program to determine the type of binding free energies contributing to the protein–ligand complex formation during MD simulation. All the complexes significantly used van der Waal's energy to form. This was followed by binding and SASA energies. Results from binding free energy calculations indicate that the formation of protein–ligand complexes is in accordance with molecular docking and dynamics simulations. Additionally, all the binding free energy calculations indicate that rutin binds effectively with all the target proteins in comparison with the control drugs. In the case of AG, rutin had the highest van der Waal's binding free energy of -324.712 kJ/mol, which was in accordance with the study conducted by Adinortey et al. (2022) [71], while binding with AM it had a van der Waal's binding free energy of -204.258 kJ/mol. The values obtained in our study were in accordance with the study by Lolok et al. (2021) for the inhibition of AM [72]. In another study, Yu et al. (2016) performed binding free energy calculations for the HSA–paclitaxel complex [73]. The results obtained from our calculations for HSA are found to be consistent with those given by Yu et al. (2016) [73]. In addition, a similar pattern of results was obtained for HAR complexed with rutin, which was found to be in accordance with Ciccone et al. (2022), where nature-inspired o-benzyl oxime-based derivatives bound with HAR were evaluated for the binding free energy calculations [74].

By the virtue of results obtained in our in vitro and in silico experiments, we propose rutin as the multi-target inhibitor of diabetes mellitus. In these experiments, it has been revealed that rutin can effectively inhibit all the enzymes (AG, AM, HSA, and HAR) effectively. Therefore, rutin would have the same effects in the in vivo studies. Rutin would decrease blood glucose levels, superoxide ions, and AGE levels. It would also reduce the production of sorbitol by interfering with the polyol pathway. Overall, it would reduce the characteristics of diabetes mellitus at different stages. While most phytochemical-based studies only focus on dual inhibition or single inhibition of target proteins [8], our study involves the inhibition of multiple proteins using a single phytochemical. Therefore, in the near future, rutin could be used as a potential inhibitor of the above-mentioned target enzymes in vivo and in clinical trials.

5. Conclusions

This study investigates the antihyperglycemic properties of the complete unripe jackfruit, as well as the polyphenol compound (rutin) that makes it up. Furthermore, MJ inhibits both the carbohydrate digesting enzymes, in addition to aldose reductase inhibition and anti-glycation potential. The extract also showed significant antioxidant activity by reducing the superoxide levels. The positive effects of MJ match those of isolated rutin, suggesting that rutin could be employed as anti-diabetic medication. Our data clearly demonstrate the antioxidant properties of MJ and rutin, proposing a link to their anti-diabetic properties. Furthermore, the presence of large levels of rutin in MJ provided support for a robust chemical basis for MJ's anti-diabetic properties. Since rutin is largely present in the extract, we propose rutin as a potential lead inhibitor of all the target enzymes used in this study. In computational studies, rutin outperformed all other phytochemicals and control drugs to become a ubiquitous inhibitor of all target proteins. Based on the findings of this investigation, a further experimental effort will hopefully be prioritized, resulting in the effective design and development of novel antihyperglycaemic drugs from different jackfruit extracts.

Supplementary Materials: The following supporting information can be downloaded at: <https://www.mdpi.com/article/10.3390/separations9090262/s1>, Figure S1: Purification outline of rutin from methanol extract of whole jackfruit flour and its structure; Figure S2: HPLC Chromatogram of standard phenolic compounds viz., (1) Ascorbic acid, (2) Gallic acid, (3) Catechin, (4) Methyl gallate, (5) Caffeic acid, (6) Syringic acid, (9) Rutin, (10) p-Coumaric acid, (11) Sinapic acid, (12) Ferrulic acid, (14) Myrecetin, (15) Quercetin, (16) Apigenin, and (17) Kaempferol (A). HPLC Chromatogram of methanol extract of whole jackfruit flour (B); Figure S3: NMR Assignments of Rutin; Figure S4: LC-MS Chromatogram of Rutin.

Author Contributions: R.R. planned and conceptualized the manuscript; T.M. and S.M.P. were involved in data analysis and method development; B.P., R.R.A., V.S. and E.S. were involved in supervision, editing and preparation of the manuscript draft. All authors have read and agreed to the published version of the manuscript.

Funding: This research received no external funding.

Institutional Review Board Statement: Not applicable.

Informed Consent Statement: Not applicable.

Data Availability Statement: Not applicable.

Acknowledgments: All the authors thank JSS Academy of Higher Education and Research (Mysore, Karnataka, India) for their kind support with the university research grant for faculty (REG/DIR (R)/URG/54/2011-12/9800), encouragement, and providing the necessary facilities.

Conflicts of Interest: All authors declare no conflict of interest.

References

1. Rachdaoui, N. Insulin: The friend and the foe in the development of type 2 diabetes mellitus. *Int. J. Mol. Sci.* **2020**, *21*, 1770. [[CrossRef](#)] [[PubMed](#)]
2. Sinha, R.; Fisch, G.; Teague, B.; Tamborlane, W.V.; Banyas, B.; Allen, K.; Savoye, M.; Rieger, V.; Taksali, S.; Barbetta, G.; et al. Prevalence of impaired glucose tolerance among children and adolescents with marked obesity. *N. Engl. J. Med.* **2002**, *346*, 802–810. [[CrossRef](#)] [[PubMed](#)]
3. Rocchini, A.P. Childhood obesity and a diabetes epidemic. *N. Engl. J. Med.* **2002**, *346*, 854–855. [[CrossRef](#)] [[PubMed](#)]
4. Tuomi, T.; Santoro, N.; Caprio, S.; Cai, M.; Weng, J.; Groop, L. The many faces of diabetes: A disease with increasing heterogeneity. *Lancet* **2014**, *383*, 1084–1094. [[CrossRef](#)]
5. Ramu, R.; Patil, S.M. A perspective on the effective conduction of functional-based coaching program on diabetic Indonesian communities. *Oman Med. J.* **2021**, *36*, e281. [[CrossRef](#)] [[PubMed](#)]
6. Harding, J.L.; Pavkov, M.E.; Magliano, D.J.; Shaw, J.E.; Gregg, E.W. Global trends in diabetes complications: A review of current evidence. *Diabetologia* **2019**, *62*, 3–16. [[CrossRef](#)]

7. Ramu, R.; Shirahatti, P.S.; Zameer, F.; Nagendra, P.M.N. Inhibitory effect of banana (*Musa* sp. var. Nanjangud rasa bale) flower extract and its constituents umbelliferone and lupeol on α -glucosidase; aldose reductase and glycation at multiple stages. *S. Afr. J. Bot.* **2014**, *95*, 54–63. [[CrossRef](#)]
8. Ramu, R.S.; Shirahatti, P.; Zameer, F.; Lakkappa, D.B.; Prasad, N.P.N. Assessment of in vivo anti-diabetic properties of umbelliferone and lupeol constituents of banana (*Musa* sp. var. Nanjangud Rasa Bale) flower in hyperglycaemic rodent model. *PLoS ONE* **2016**, *11*, e0151135.
9. Tang, W.; Martin, K.A.; Hwa, J. Aldose reductase, oxidative stress, and diabetic mellitus. *Front. Pharmacol.* **2012**, *3*, 87. [[CrossRef](#)]
10. Jannapureddy, S.; Sharma, M.; Yepuri, G.; Schmidt, A.M.; Ramasamy, R. Aldose reductase: An emerging target for development of interventions for diabetic cardiovascular complications. *Front. Endocrinol.* **2021**, *12*, 636267. [[CrossRef](#)]
11. Singh, V.P.; Bali, A.; Singh, N.; Jaggi, A.S. Advanced glycation end products and diabetic complications. *Korean. J. Physiol. Pharmacol.* **2014**, *18*, 1–4. [[CrossRef](#)] [[PubMed](#)]
12. Rungratanawanich, W.; Qu, Y.; Wang, X.; Essa, M.M.; Song, B.J. Advanced glycation end products (AGEs) and other adducts in aging-related diseases and alcohol-mediated tissue injury. *Exp. Mol. Med.* **2021**, *53*, 168–188. [[CrossRef](#)] [[PubMed](#)]
13. Prathapan, A.; Nampoothiri, S.V.; Mini, S.; Raghu, K.G. Antioxidant, antiglycation and inhibitory potential of *Saraca ashoka* flowers against the enzymes linked to type 2 diabetes and LDL oxidation. *Eur. Rev. Med. Pharmacol. Sci.* **2012**, *16*, 57–65. [[PubMed](#)]
14. Patil, S.M.; Shirahatti, P.S.; Ramu, R. *Azadirachta indica* A. Juss (neem) against diabetes mellitus: A critical review on its phytochemistry, pharmacology, and toxicology. *J. Pharm. Pharmacol.* **2022**, *74*, 681–710. [[CrossRef](#)]
15. Patil, S.M.; Kumari, V.C.; Sumana, K.; Sujay, S.; Tejaswini, M.; Shirahatti, P.S.; Ramu, R. Sustainable development of plant tissue culture industry: The Indian scenario. *J. Appl. Biol. Biotechnol.* **2021**, *9*, 18–27.
16. Patil, S.M.; Ramu, R.; Shirahatti, P.S.; Shivamallu, C.; Amachawadi, R.G. A systematic review on ethnopharmacology; phytochemistry and pharmacological aspects of *Thymus vulgaris* Linn. *Heliyon* **2021**, *7*, e07054. [[CrossRef](#)]
17. Patil, S.M.; Shirahatti, P.S.; Kumari, V.B.C.; Ramu, R.; Prasad, N. *Azadirachta indica* A. Juss (neem) as a contraceptive: An evidence-based review on its pharmacological efficiency. *Phytomedicine* **2021**, *88*, 153596. [[CrossRef](#)]
18. Pushpa, V.H.; Jayanthi, M.K.; Rashmi, H.R.; Shivamurthy, V.K.; Patil, S.M.; Shirahatti, P.S.; Ramu, R. New insights on the phytochemical intervention for the treatment of neuropsychiatric disorders using the leaves of *Michelia champaca*: An in vivo and in silico approach. *Pharm Biol.* **2022**, *60*, 1656–1668.
19. Mozaffarian, D. Dietary and policy priorities for cardiovascular disease, diabetes, and obesity: A comprehensive review. *Circulation* **2016**, *133*, 187–225. [[CrossRef](#)]
20. Maradesha, T.; Patil, S.M.; Al-Mutairi, K.A.; Ramu, R.; Madhunapantula, S.V.; Alqadi, T. Inhibitory effect of polyphenols from the whole green jackfruit flour against α -glucosidase, α -amylase, aldose reductase and glycation at multiple stages and their interaction: Inhibition kinetics and molecular simulations. *Molecules* **2022**, *27*, 1888. [[CrossRef](#)]
21. Baliga, M.S.; Shivashankara, A.R.; Haniadka, R.; Dsouza, J.; Bhat, H.P. Phytochemistry; nutritional and pharmacological properties of *Artocarpus heterophyllus* Lam. (jackfruit): A review. *Food Res. Int.* **2011**, *44*, 1800–1811. [[CrossRef](#)]
22. Swami, S.B.; Thakor, N.J.; Haldankar, P.M.; Kalse, S.B. Jackfruit and its many functional components as related to human health: A review. *Compr. Rev. Food Sci. Food Saf.* **2012**, *11*, 565–576. [[CrossRef](#)]
23. Razali, N.; Razab, R.; Junit, S.M.; Aziz, A.A. Radical scavenging and reducing properties of extracts of cashew shoots (*Anacardium occidentale*). *Food. Chem.* **2008**, *111*, 38–44. [[CrossRef](#)]
24. Seal, T. Quantitative HPLC analysis of phenolic acids; flavonoids and ascorbic acid in four different solvent extracts of two wild edible leaves; *Sonchus arvensis* and *Oenanthe linearis* of North-Eastern region in India. *J. Appl. Pharm. Sci.* **2016**, *6*, 157–166. [[CrossRef](#)]
25. Ordon-Ez, A.A.; Gomez, J.D.; Vattuone, M.A.; Isla, M.I. Antioxidant activities of *Sechiumedule* (Jacq.) Swart extracts. *Food Chem.* **2006**, *97*, 452–458. [[CrossRef](#)]
26. Shuxia, C.; Xiaoqing, S.; Siqiong, C.; Panpan, L.; Junna, D.; Yanxia, C.; Huanwen, M. Evaluation of garlic cultivars for polyphenolic content and antioxidant properties. *PLoS ONE* **2013**, *8*, e79730.
27. Harbone, J.B. *Phytochemical Methods*, 1st ed.; Chapman and Hall Ltd.: London, UK, 1973; pp. 49–188.
28. Patil, S.M.; Martiz, R.M.; Ramu, R.; Shirahatti, P.S.; Prakash, A.; Kumar, B.P.; Kumar, N. Evaluation of flavonoids from banana pseudostem and flower (quercetin and catechin) as potent inhibitors of α -glucosidase: An in-silico perspective. *J. Biomol. Struct. Dyn.* **2021**, *7*, 1–5. [[CrossRef](#)]
29. Shivanna, C.; Patil, S.M.; Mallikarjunaswamy, M.; Ramu, R.; Akhileshwari, P.; Nagaraju, L.R.; Sridhar, M.A.; Khanum, S.A.; Ranganatha, L.; Silina, E.; et al. Synthesis, characterization, Hirschfeld surface analysis, crystal structure and molecular modeling studies of 1-(4-(Methoxy(phenyl)methyl)-2-methylphenoxy)butan-2-one derivative as a novel α -glucosidase inhibitor. *Crystals* **2022**, *12*, 960. [[CrossRef](#)]
30. Martiz, R.M.; Patil, S.M.; Ramu, R.; Mallappa Kumar, J.; Ranganatha, L.V.; Khanum, S.A.; Silina, E.; Stupin, V.; Achar, R.R. Discovery of novel benzophenone integrated derivatives as anti-Alzheimer's agents targeting presenilin-1 and presenilin-2 inhibition: A computational approach. *PLoS ONE* **2022**, *17*, e0265022. [[CrossRef](#)]
31. Patil, S.M.; Martiz, R.M.; Ramu, R.; Shirahatti, P.S.; Prakash, A.; Chandra, J.S.; Ranganatha, L.V. In silico identification of novel benzophenone-coumarin derivatives as SARS-CoV-2 RNA dependent RNA polymerase (RdRp) inhibitors. *J. Biomol. Struct. Dyn.* **2021**, *11*, 1–17. [[CrossRef](#)]

32. Kumar, V.; Shetty, P.; Arunodaya, H.S.; Chandra, K.S.; Ramu, R.; Patil, S.M.; Baliga, A.; Rai, V.M.; Shalini Shenoy, M.; Udipi, V.; et al. Potential fluorinated anti-MRSA thiazolidinone derivatives with antibacterial, antitubercular activity and molecular docking studies. *Chem. Biodivers.* **2022**, *19*, e202100532. [[CrossRef](#)] [[PubMed](#)]
33. Sajal, H.; Patil, S.M.; Raj, R.; Shbeer, A.M.; Ageel, M.; Ramu, R. Computer-aided screening of phytoconstituents from *ocimum tenuiflorum* against diabetes mellitus targeting dpp4 inhibition: A combination of molecular docking, molecular dynamics, and pharmacokinetics approaches. *Molecules* **2022**, *27*, 5133. [[CrossRef](#)] [[PubMed](#)]
34. Gurupadaswamy, H.D.; Ranganatha, V.L.; Ramu, R.; Patil, S.M.; Khanum, S.A. Competent synthesis of biaryl analogs via asymmetric Suzuki–Miyaura cross-coupling for the development of anti-inflammatory and analgesic agents. *J. Iran. Chem. Soc.* **2022**, *1*, 2421–2436. [[CrossRef](#)]
35. Patil, S.M.; Maruthi, K.R.; Bajpe, N.S.; Vyshali, V.M.; Sushmitha, S.; Chagalamari, A.; Ramith, R. Comparative molecular docking and simulation analysis of molnupiravir and remdesivir with SARS-CoV-2 RNA dependent RNA polymerase (RdRp). *Bioinformation* **2021**, *7*, 932–939.
36. Martiz, R.M.; Patil, S.M.; Abdulaziz, M.; Babalghith, A.; Al-Areefi, M.; Al-Ghorbani, M.; Mallappa Kumar, J.; Prasad, A.; Mysore Nagalingaswamy, N.P.; Ramu, R. Defining the Role of Isoeugenol from *Ocimum tenuiflorum* against Diabetes Mellitus-Linked Alzheimer’s Disease through Network Pharmacology and Computational Methods. *Molecules* **2022**, *27*, 2398. [[CrossRef](#)]
37. Shukla, P.; Gopalkrishna, B.; Shukla, P. Isolation of rutin from *Phyllanthus amarus*. *Int. J. Pharm. Sci. Res.* **2012**, *3*, 1198–1201.
38. Lin, L.J.; Huang, X.B.; Lv, Z.C. Isolation and identification of flavonoids components from *Pteris vittata* L. *Springer Plus.* **2016**, *5*, 1649. [[CrossRef](#)]
39. D’Aiuto, F.; Gkranias, N.; Bhowruth, D.; Khan, T.; Orlandi, M.; Suvan, J.; Masi, S.; Tsakos, G.; Hurel, S.; Hingorani, A.D.; et al. Systemic effects of periodontitis treatment in patients with type 2 diabetes: A 12 month, single-centre, investigator-masked, randomised trial. *Lancet. Diabetes. Endocrinol.* **2018**, *6*, 954–965. [[CrossRef](#)]
40. Zafar, A.; Alruwaili, N.K.; Panda, D.S.; Imam, S.S.; Alharbi, K.S.; Afzal, M.; Shalaby, K.; Kazmi, I.; Alshehri, S. Potential of Natural Bioactive Compounds in Management of Diabetes: Review of Preclinical and Clinical Evidence. *Curr. Pharmacol. Rep.* **2021**, *7*, 107–122. [[CrossRef](#)]
41. Piña-Contreras, N.; Martínez-Moreno, A.G.; Ramírez-Anaya, J.D.P.; Espinoza-Gallardo, A.C.; Valdés, E.H.M. Raspberry (*Rubus idaeus* L.), a Promising Alternative in the Treatment of Hyperglycemia and Dyslipidemias. *J. Med. Food.* **2022**, *25*, 121–129. [[CrossRef](#)]
42. Savych, A.; Milian, I. Total flavonoid content in the herbal mixture with anti-diabetic activity. *PharmacologyOnLine* **2021**, *2*, 68–75.
43. Chen, L.Y.; Huang, C.N.; Liao, C.K.; Chang, H.M.; Kuan, Y.H.; Tseng, T.J.; Yen, K.J.; Yang, K.L.; Lin, H.C. Effects of rutin on wound healing in hyperglycemic rats. *Antioxidants* **2020**, *9*, 1122. [[CrossRef](#)] [[PubMed](#)]
44. Barik, S.K.; Russell, W.R.; Moar, K.M.; Cruickshank, M.; Scobbie, L.; Duncan, G.; Hoggard, N. The anthocyanins in black currants regulate postprandial hyperglycaemia primarily by inhibiting α -glucosidase while other phenolics modulate salivary α -amylase, glucose uptake and sugar transporters. *J. Nutr. Biochem.* **2020**, *78*, 108325. [[CrossRef](#)]
45. Dubey, S.; Ganeshpurkar, A.; Ganeshpurkar, A.; Bansal, D.; Dubey, N. Glycolytic enzyme inhibitory and antiglycation potential of rutin. *Future. J. Pharm. Sci.* **2017**, *3*, 158–162. [[CrossRef](#)]
46. Tadera, K.; Minami, Y.; Takamatsu, K.; Matsuoka, T. Inhibition of α -glucosidase and α -amylase by flavonoids. *J. Nutr. Sci. Vitaminol.* **2006**, *52*, 149–153. [[CrossRef](#)]
47. Niimi, N.; Yako, H.; Takaku, S.; Chung, S.K.; Sango, K. Aldose Reductase and the polyol pathway in schwann cells: Old and new problems. *Int. J. Mol. Sci.* **2021**, *22*, 1031. [[CrossRef](#)]
48. Kumar, A.A.; Satheesh, G.; Vijayakumar, G.; Chandran, M.; Prabhu, P.R.; Simon, L.; Kutty, V.R.; Kartha, C.C.; Jaleel, A. Postprandial metabolism is impaired in overweight normoglycemic young adults without family history of diabetes. *Sci. Rep.* **2020**, *10*, 353. [[CrossRef](#)] [[PubMed](#)]
49. Benlarbi, M.; Jemai, H.; Hajri, K.; Mbarek, S.; Amri, E.; Jebbari, M.; Hammoun, I.; Baccouche, B.; Boudhrioua Mihoubi, N.; Zemmal, A.; et al. Neuroprotective effects of oleuropein on retina photoreceptors cells primary culture and olive leaf extract and oleuropein inhibitory effects on aldose reductase in a diabetic model: Meriones shawi. *Arch. Physiol. Biochem.* **2020**, *1*, 593–600. [[CrossRef](#)]
50. Hussain, T.; Tan, B.; Murtaza, G.; Liu, G.; Rahu, N.; Kalhor, M.S.; Kalhor, D.H.; Adebowale, T.O.; Mazhar, M.U.; ur Rehman, Z.; et al. Flavonoids and type 2 diabetes: Evidence of efficacy in clinical and animal studies and delivery strategies to enhance their therapeutic efficacy. *Pharmacol. Res.* **2020**, *152*, 104629. [[CrossRef](#)]
51. Dariya, B.; Nagaraju, G.P. Advanced glycation end products in diabetes, cancer and phytochemical therapy. *Drug Discov. Today* **2020**, *25*, 1614–1623. [[CrossRef](#)]
52. Fournet, M.; Bonté, F.; Desmoulière, A. Glycation damage: A possible hub for major pathophysiological disorders and aging. *Aging. Dis.* **2018**, *9*, 880. [[CrossRef](#)] [[PubMed](#)]
53. Cepas, V.; Collino, M.; Mayo, J.C.; Sainz, R.M. Redox signaling and advanced glycation endproducts (AGEs) in diet-related diseases. *Antioxidants* **2020**, *9*, 142. [[CrossRef](#)] [[PubMed](#)]
54. Zhou, J.; Zhang, L.; Li, Q.; Jin, W.; Chen, W.; Han, J.; Zhang, Y. Simultaneous optimization for ultrasound-assisted extraction and antioxidant activity of flavonoids from *Sophora flavescens* using response surface methodology. *Molecules* **2018**, *24*, 112. [[CrossRef](#)] [[PubMed](#)]

55. Patil, S.M.; Al-Mutairi, K.A.; Firdose, N.; Ramu, R.; Martiz, R.M.; Ashwini, P. Pharmacoinformatics based screening discovers swertianolin from *Lavandula angustifolia* as a novel neuromodulator targeting epilepsy, depression, and anxiety. *South. Afr. J. Bot.* **2022**, *149*, 712–730. [[CrossRef](#)]
56. Jyothi, M.; Khamees, H.A.; Patil, S.M.; Ramu, R.; Khanum, S.A. Microwave-assisted synthesis, characterization, docking studies and molecular dynamic of some novel phenyl thiazole analogs as xanthine oxidase inhibitor. *J. Iran. Chem. Soc.* **2022**, *10*, 1–5. [[CrossRef](#)]
57. Shahzad, D.; Saeed, A.; Larik, F.A.; Channar, P.A.; Abbas, Q.; Alajmi, M.F.; Arshad, M.I.; Erben, M.F.; Hassan, M.; Raza, H.; et al. Novel C-2 symmetric molecules as α -glucosidase and α -amylase inhibitors: Design; synthesis; kinetic evaluation; molecular docking and pharmacokinetics. *Molecules* **2019**, *24*, 1511. [[CrossRef](#)]
58. Ganavi, D.; Ramu, R.; Kumar, V.; Patil, S.M.; Martiz, R.M.; Shirahatti, P.S.; Sathyanarayana, R.; Poojary, B.; Holla, B.S.; Poojary, V.; et al. In vitro and in silico studies of fluorinated 2; 3-disubstituted thiazolidinone-pyrazoles as potential α -amylase inhibitors and antioxidant agents. *Arch. Pharm.* **2021**, *12*, e2100342. [[CrossRef](#)]
59. Osman, W.; Ismail, E.M.; Shantier, S.W.; Mohammed, M.S.; Mothana, R.A.; Muddathir, A.; Khalid, H.S. In silico assessment of potential leads identified from *Bauhinia rufescens* Lam. as α -glucosidase and α -amylase inhibitors. *J. Recept. Signal Transduct. Res.* **2021**, *41*, 159–169. [[CrossRef](#)]
60. Jhong, C.H.; Riyaphan, J.; Lin, S.H.; Chia, Y.C.; Weng, C.F. Screening alpha-glucosidase and alpha-amylase inhibitors from natural compounds by molecular docking in silico. *Biofactors* **2015**, *41*, 242–251. [[CrossRef](#)]
61. Isogai, H.; Hirayama, N. In silico prediction of interactions between site II on human serum albumin and profen drugs. *Int. Sch. Res. Not.* **2013**, *2013*, 818364. [[CrossRef](#)]
62. Ghuman, J.; Zunszain, P.A.; Petitpas, I.; Bhattacharya, A.A.; Otagiri, M.; Curry, S. Structural basis of the drug-binding specificity of human serum albumin. *J. Mol. Biol.* **2005**, *353*, 38–52. [[CrossRef](#)] [[PubMed](#)]
63. Ali, M.S.; Al-Lohedan, H.A. Experimental and Computational Investigation on the Interaction of Anticancer Drug Gemcitabine with Human Plasma Protein: Effect of Copresence of Ibuprofen on the Binding. *Molecules* **2022**, *27*, 1635. [[CrossRef](#)] [[PubMed](#)]
64. Ramu, R.; Shirahatti, P.S.; Deepika, T.H.; Bajpe, S.N.; Sreepathi, N.; Patil, S.M.; Prasad, N. Investigating *Musa paradisiaca* (Var. Nanjangud rasa bale) pseudostem in preventing hyperglycemia along with improvement of diabetic complications. *J. Appl. Biol. Biotechnol.* **2022**, *10*, 56–65. [[CrossRef](#)]
65. Kufareva, I.; Abagyan, R. Methods of protein structure comparison. *Methods Mol. Biol.* **2012**, *857*, 231–257. [[PubMed](#)]
66. Medina-Franco, J.L.; Méndez-Lucio, O.; Martinez-Mayorga, K. The interplay between molecular modeling and chemoinformatics to characterize protein–ligand and protein–protein interactions landscapes for drug discovery. *Adv. Protein Chem. Struct. Biol.* **2014**, *96*, 1–37. [[PubMed](#)]
67. Kumar, V.; Ramu, R.; Shirahatti, P.S.; Kumari, V.C.; Sushma, P.; Mandal, S.P.; Patil, S.M. α -glucosidase, α -amylase inhibition, kinetics and docking studies of novel (2-chloro-6-(trifluoromethyl)benzyloxy) arylidene based rhodanine and rhodanine acetic acid derivatives. *ChemistrySelect* **2021**, *6*, 9637–9644. [[CrossRef](#)]
68. Soltanabadi, O.; Atri, M.S.; Bagheri, M. Spectroscopic analysis; docking and molecular dynamics simulation of the interaction of cinnamaldehyde with human serum albumin. *J. Incl. Phenom. Macrocycl. Chem.* **2018**, *91*, 189–197. [[CrossRef](#)]
69. Radibratovic, M.; Minic, S.; Stanic-Vucinic, D.; Nikolic, M.; Milcic, M.; CirkovicVelickovic, T. Stabilization of human serum albumin by the binding of phycocyanobilin; a bioactive chromophore of blue-green alga *Spirulina*: Molecular dynamics and experimental study. *PLoS ONE* **2016**, *11*, e0167973. [[CrossRef](#)]
70. Tanawattanasuntorn, T.; Thongpanchang, T.; Rungrotmongkol, T.; Hanpaibool, C.; Graidist, P.; Tipmanee, V. (–)-Kusunokinin as a Potential AR Inhibitor: Equivalency Observed via AKR1B1 Dynamics Simulation. *ACS Omega* **2020**, *6*, 606–614. [[CrossRef](#)]
71. Adinortey, C.A.; Kwarko, G.B.; Koranteng, R.; Boison, D.; Obuaba, I.; Wilson, M.D.; Kwofie, S.K. Molecular Structure-Based Screening of the Constituents of *Calotropis procera* Identifies Potential Inhibitors of Diabetes Mellitus Target Alpha Glucosidase. *Curr. Issues Mol. Biol.* **2022**, *44*, 963–987. [[CrossRef](#)]
72. Lolok, N.; Sumiwi, S.A.; Muhtadi, A.; Susilawati, Y.; Hendriani, R.; Ramadhan, D.S.; Levita, J.; Sahidin, I. Molecular docking and molecular dynamics studies of bioactive compounds contained in noni fruit (*Morinda citrifolia* L.) against human pancreatic α -amylase. *J. Biomol. Struct. Dyn.* **2021**, *3*, 7091–7098. [[CrossRef](#)] [[PubMed](#)]
73. Yu, H.; Li, D.; Xu, F.; Pan, Q.; Chai, P.; Liu, B.; Chen, C. The binding affinity of human serum albumin and paclitaxel through MMPBSA based on docked complex. *Mol. Simul.* **2016**, *42*, 1460–1467. [[CrossRef](#)]
74. Ciccone, L.; Petrarolo, G.; Barsuglia, F.; Fruchart-Gaillard, C.; Cassar Lajeunesse, E.; Adewumi, A.T.; Soliman, M.E.S.; La Motta, C.; Orlandini, E.; Nencetti, S. Nature-Inspired O-Benzyl Oxime-Based Derivatives as New Dual-Acting Agents Targeting Aldose Reductase and Oxidative Stress. *Biomolecules* **2022**, *12*, 448. [[CrossRef](#)] [[PubMed](#)]